1.0   2.8 2.5

       3.2 2.2

            2.0

1.1   1.8

1.25 1.4 1.6

LEVEL II (12)

R–1433

MATERIALS RESEARCH FOR ADVANCED
INERTIAL INSTRUMENTATION

TASK 1: DIMENSIONAL STABILITY OF
GYROSCOPE STRUCTURAL MATERIALS

DECEMBER 1980

DTIC
SELECTE
APR 24 1981

E

TECHNICAL REPORT NO. 3
FOR THE PERIOD
1 OCTOBER 1979–30 SEPTEMBER 1980

BY

K. KUMAR, J. McCARTHY, F. PETRI, J. WOLLAM

The Charles Stark Draper Laboratory, Inc.
Cambridge, Massachusetts 02139

81 4 24 043

REPORT DOCUMENTATION PAGE		READ INSTRUCTIONS BEFORE COMPLETING FORM
1. REPORT NUMBER R-1433	2. GOVT ACCESSION NO AD-A098165	3. RECIPIENT'S CATALOG NUMBER
4. TITLE *(and Subtitle)* Materials Research for Advanced Inertial Instrumentation, Task 1, Dimensional Stability of Gyro Structural Materials		5. TYPE OF REPORT & PERIOD COVERED
		6. PERFORMING ORG. REPORT NUMBER
7. AUTHOR(s) K. Kumar, J. McCarthy, F. Petri, J. Wollam		8. CONTRACT OR GRANT NUMBER(s) N00014-77-C-0388
9. PERFORMING ORGANIZATION NAME AND ADDRESS The Charles Stark Draper Laboratory, Inc. 555 Technology Square Cambridge, Massachusetts 02139		10. PROGRAM ELEMENT, PROJECT, TASK AREA & WORK UNIT NUMBERS
11. CONTROLLING OFFICE NAME AND ADDRESS Office of Naval Research Department of the Navy 800 N. Quincy Street, Arlington, Virginia 22217		12. REPORT DATE December 1980
		13. NUMBER OF PAGES 76
14. MONITORING AGENCY NAME & ADDRESS *(if different from Controlling Office)* Office of Naval Research-Boston Branch 666 Summer Street Boston, Massachusetts 02210		15. SECURITY CLASS. *(of this report)* UNCLASSIFIED
		15a. DECLASSIFICATION/DOWNGRADING SCHEDULE

16. DISTRIBUTION STATEMENT *(of this Report)*

Approved for public release, distribution unlimited.

17. DISTRIBUTION STATEMENT *(of the abstract entered in Block 20, if different from Report)*

18. SUPPLEMENTARY NOTES

19. KEY WORDS *(Continue on reverse side if necessary and identify by block number)*

Dimensional Stability	Microcreep
Finite Element Analysis	Micromechanical Properties
Gyroscope Materials	Microstrain Modeling
Hot Isostatically Pressed Beryllium	Microyield Strength
Instrument Materials	Optical and Electron Microscopy

20. ABSTRACT *(Continue on reverse side if necessary and identify by block number)*

Additional microyield measurements on HIP-50 beryllium samples, subjected to a variety of selected heat treatments, were performed. It was determined that of the several treatments that were employed the most significant increase in the value of the microyield strength occurred from a 100 hour exposure to 600°C. A microyield value of about 26.5 klb/in² was measured after this treatment compared to an as-received value of 17.2 klb/in². Examination of the microyield data plotted on logarithmic coordinates showed that if a

DD FORM 1473 EDITION OF 1 NOV 65 IS OBSOLETE
1 JAN 73

correlation is desired between the processes of microyield and microcreep, one must take into account the value of the strain exponent (which is the slope of the straight line) in the low strain regime, in addition to the measured value of the microyield strength. Experiments performed in this study showed that considerable care should be exercised in the preparation of samples for microstructure examination to avoid introducing mechanical damage in regions near the surface. Optical microscopy was found to have limited utility in determining the effects of the several thermal treatments on sample micro-structure. Transmission electron microscopy, however, was successfully performed after jet-thinning the samples in a chromic-acetic acid electrolyte. The differences observed were mainly related to phase precipitation and segregation. Attempts to identify these precipitates are planned for the future.

A brief review of the creep modelling work performed to date under this program is included in this report. As a continuation of this effort a finite element analysis of a proposed CSDL test specimen for microcreep measurement was completed. Initally a specimen with axisymmetric ribs for mounting the creep measurement fixturing was proposed. The analysis showed that these ribs cause disturbances in the uniform stress field which extend far into the specimen. A dramatic reduction can be achieved by replacing each rib with three individual lugs.

R-1433

MATERIALS RESEARCH FOR ADVANCED INERTIAL INSTRUMENTATION

TASK 1: DIMENSIONAL STABILITY OF GYRO STRUCTURAL MATERIALS

DECEMBER 1980

TECHNICAL REPORT NO.3

FOR THE PERIOD

1 October 1979 - 30 September 1980

K. Kumar, J. McCarthy, F. Petri, J. Wollam

Prepared for the Office of Naval Research,
Department of the Navy, under Contract N00014-78-C-0388.

Approved: _M.S. Sapuppo_
M.S. Sapuppo, Head
Component Development Department

The Charles Stark Draper Laboratory
Cambridge, Massachusetts 02139

ACKNOWLEDGEMENTS

TABLE OF CONTENTS

iii

LIST OF ILLUSTRATIONS

LIST OF ILLUSTRATIONS (Continued)

LIST OF TABLES

SECTION 1

INTRODUCTION

Micromechanical processes leading to small mass shifts are very important to the designer of inertial instruments. These mass shifts are associated with dimensional changes that different parts of the instrument experience during different modes of operation and assembly. The most common causes of dimensional instability in structural materials usually are phase transformation, relief of residual stresses, and microplastic deformation from applied stresses. Although effects related to phase transformations and residual stresses can generally be controlled effectively through proper alloy and process selection procedures, those related to applied stresses are more difficult to control because some minimum stresses are in fact needed for proper functioning of the inertial instruments.

As greater demands are made on the accuracy of measuring devices, microplastic strains on the order of 10^{-6} and 10^{-7} become significant sources of instrument error. Strains of this order of magnitude have been found to occur at relatively low stresses in moderate strength engineering materials under the action of essential assembly operations such as shrink fit, bolt tension, or rotational stress. Since it is not possible to reduce these assembly stresses below a reasonable limit, it becomes desirable to predict the plastic microstrain and compensate for the resulting errors. For evaluation purposes, the designer frequently uses the microyield strength of the material as a guideline in assessing its short-term and long-term performance inside the device of interest. A microyield strength measurement typically consists of a series of short-term load-unload cycles, increasing in stress level. During this period the total accumulated residual plastic strain is recorded for each incrementally higher level of applied stress.

Conventionally, that level of applied stress which is required to result in one residual microstrain (= 10^{-6} strain) is referred to as the microyield strength of the material [1].

While the significance of the microyield strength of the material in terms of short-term strain effects is seemingly apparent, its role in defining long-term performance is not as clear. Long-term processes of microcreep (creep at the 10^{-6} level) may or may not be directly, or even indirectly, related to the microyield strength value. In fact, recent observations elsewhere [2] indicate that microcreep will occur at stress levels which are only a small fraction of the microyield strength value. However, in lieu of available, reliable, microcreep data on the materials of interest (because of the very long time intervals and much sophisticated instrumentation that are required to collect it), device designers have acted on the premise that a higher microyield strength material will also be more resistant to long-term effects of microcreep. Such a relationship between microyield and microcreep, if it exists, would be also of great interest to the materials engineer, principally because, by performing short-term microyielding experiments, one could conceivably predict long-term microcreep behavior. This would permit a much quicker evaluation of the materials of interest. A major area of emphasis in this activity until now has been the experimental determination of microyield properties of HIP-50 (hot isostatically pressed) beryllium. By performing these experiments we have obtained considerably more insight than previously existed into the significance of microyield data and its interpretation. This increased understanding is expected to permit the development of a closer correlation between the processes of microyield and microcreep than would otherwise have been possible.

SECTION 2

OBJECTIVES

The principal objectives of this program have been as follows:

(1)   To survey the literature on microplastic properties of
        materials and summarize the data for use in modelling
        instrument performance and design analysis. (This
        information was contained in reference (3).)

(2)   To study the microplastic behavior of HIP beryllium and
        the relationship to microstructure.

(3)   To predict microdeformation behavior of typical instrument
        components using finite element analysis techniques and
        experimentally determined microcreep data.

SECTION 3

PREVIOUS WORK

Work accomplished during the first two years of this effort is described in detail in references (3) and (4). A brief summary is presented below.

(1)   Hot isostatically pressed beryllium was purchased from Kawecki Berylco Industries. (HIP-50 is their designation.)

(2)   A procedure was established for preparing tensile specimens for microyield strength tests and for applying strain gages for measuring microstrain.

(3)   Methods for measuring misalignment in loading were investigated and a load train was modified to provide a reasonable precision of alignment.

(4)   Microyield strength measurements were performed with strict temperature control on as-pressed and 1080°F, 100 hours heat-treated HIP-50 samples.

(5)   An initial microstructure examination was made of the as-pressed HIP-50 material by R. Polvani of the National Bureau of Standards using transmission electron microscopy.

(6)   Modeling studies were performed on a typical gyro component and on a disc-shaped specimen for biaxial loading. Deflection, resulting from microcreep processes, was calculated for these instances.

5

SECTION 4

PRESENT WORK

Most of this past year's activity has been concerned with collection of additional microyield strength data, microstructure examination of selected samples at different conditions of heat treatment using both optical and transmission electron microscopy, and further extension of microcreep modeling efforts on structural components. These activities will be discussed separately in greater detail.

4.1   Heat Treatment of Samples

Two of the heat treatments used for HIP 50 involved temperatures of 870°C and 1055°C. Ordinarily, beryllium is heat treated in a protective atmosphere to prevent oxidation. However, above 850°C the vapor pressure of beryllium becomes sufficiently high to cause concern about furnace contamination. In order to contain any vaporized beryllium both heat treatments were performed with the specimen blanks sealed in stainless steel containers. The containers were made from seamless tubing with welded end caps. In use, the loaded container was evacuated and back-filled with a partial pressure of inert gas through an evacuation tube in the end cap, after which the tube was crimped and welded shut. The 870°C heat treatment was performed in a tube furnace with argon at atmospheric pressure, while the 1055°C heat treatment was done in a vacuum furnace with 200 micron partial pressure of argon.

4.2   Results of Microyield Strength Measurements

The apparatus used for conducting the microyield stress tests is shown in Figure 1, which depicts the instrumented specimen and load

7
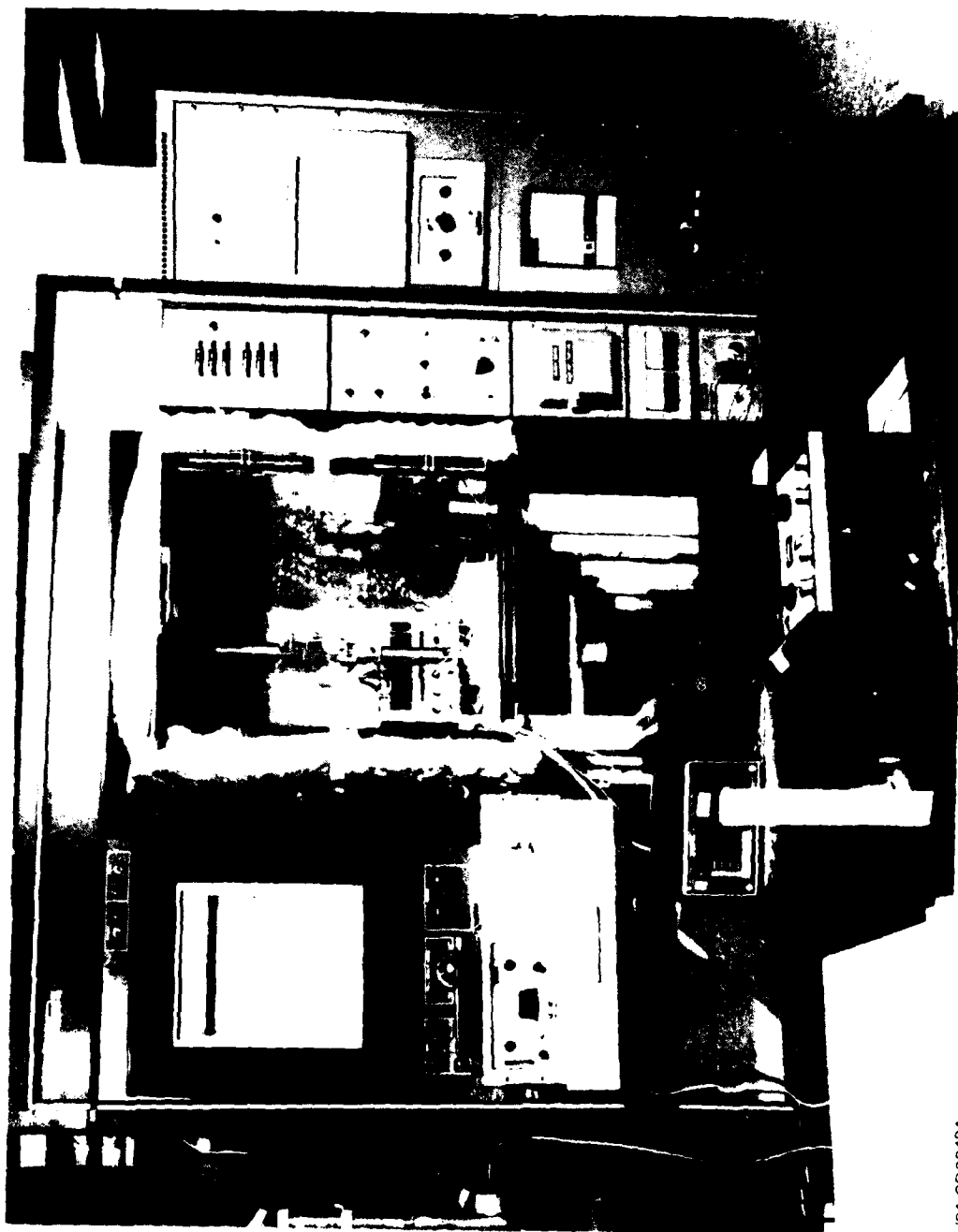
Figure 1. Equipment for microyield testing.

1/81 CD22481

16

train mounted in an Instron tensile machine. The load train was carefully installed in the testing machine to avoid any effects of friction or bending. With the load train design shown in Figure 2, the typical precision of alignment was 3×10^{-4}. This corresponded to an extreme fiber bending stress of 1.3 klb/in^2 at 5.0 klb/in^2 average stress. While this was considered only moderately good alignment, the experiments were continued because any further improvement in alignment would have necessitated a major redesign of the aligning fixture. Resistance strain gages were used to measure the level of strain induced in the material. More details on the apparatus and the measuring equipment can be obtained from Reference (4).

Before starting a test, the specimen and instrumentation were set up and the instruments allowed to run overnight to establish temperature equilibrium. The specimen was then loaded to a low stress, approximately 2 klb/in^2, and unloaded and reloaded several times to determine the repeatability of the unstrained zero reading. After this initial evaluation, the run was performed with the specimen being loaded and unloaded to increasing values of the applied stress, and the values of loaded and unloaded strain recorded. Strain rate was 0.008 inch/inch/minute for both loading and unloading. Load was maintained for 30 seconds. When the specimen was in the fully unloaded state, the crosshead in the load train was moved at high speed to establish 0.030-inch clearance between the pin and the lower pull rod. After a 1-minute interval, the unloaded strain data were printed out and the specimen was reloaded. In conventional manner the recorded data were plotted, with the applied stress on the vertical axis and the measured residual strain on the horizontal axis of a linear graph paper. Curves, similar to those shown earlier in Reference (4), were generated in each instance. The value of the applied stress corresponding to a residual strain of 1×10^{-6} on this curve constituted the microyield strength of the material, by definition. The different microyield values measured this way for the differently heat-treated samples are listed in Table I. These particular thermal treatments (which are also shown in Table I) were the result of recommendations
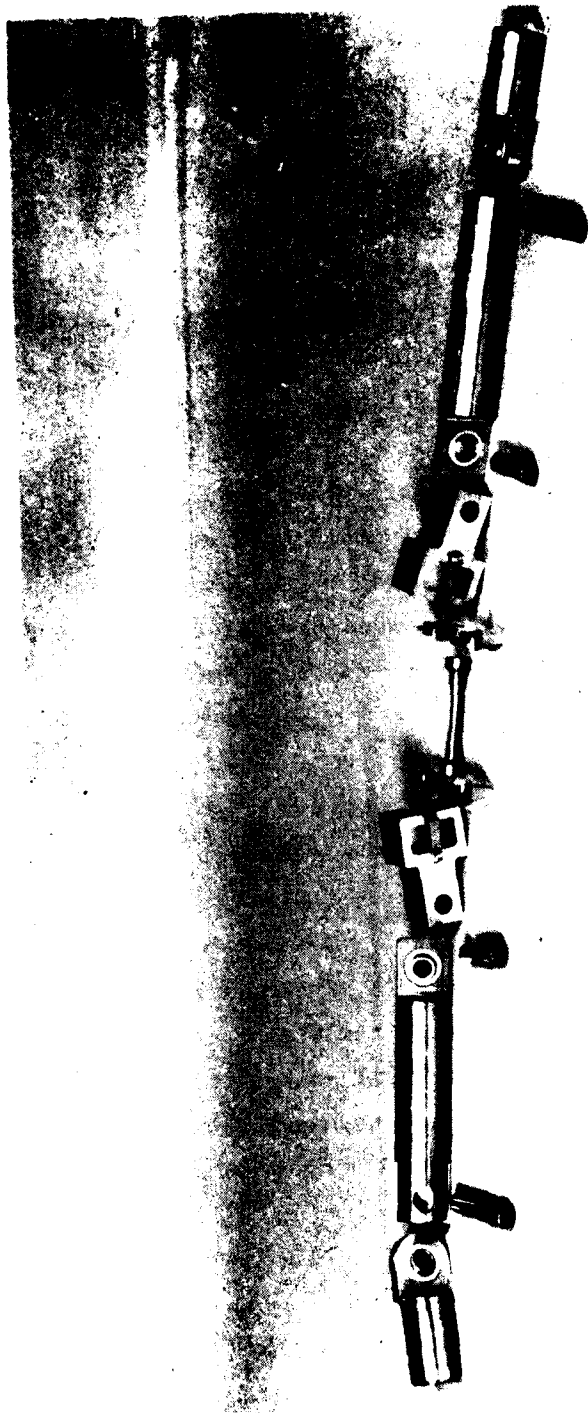
Figure 2. Load train used for measurements.

1/81 CD22482

10

Table I. Microyield strength values in klb/in^2 for differently heat-treated HIP-50 material at 27°C.

As-HIP	Heat Treatments		
	HT1	HT2	HT3
17.2	26.5	17.5	21.0

HT1: HIP + 600°C, 100 h

HT2: HIP + 1055°C, 2 h solutionize, quench + 370°C, 24 h, furnace cool

HT3: HIP + 870°C, 2 h + slow cool and step age (750°C,

20 h + 720°C, 20 h + 695°C, 20 h, furnace cool)

from an earlier, reasonably extensive study of the strengthening processes in beryllium [5].

4.3   Discussions of Microyield Strength Measurements

The selection of the value of the applied stress that corresponds to 10^{-6} strain, as the designated microyield strength of the material, is totally arbitrary [1]. One could as well define similar microyield values at 10^{-5}, 10^{-7}, 10^{-8}, or at any other level of preassigned value of residual strain. Much, of course, is dependent on the level and accuracy of the measuring apparatus available to the investigator. To gain further insight into the significance of microyield and its measurement, we decided to replot the microyield data on a log-log graph paper. Elsewhere, [1] it has been shown that in some cases, a straight line fit can be made to the data by following such a procedure. In such instances the stress-strain relationship (in the realm of low residual strain levels) can be empirically expressed as

$$\sigma = A\epsilon^n \quad (\text{for } \epsilon' \leqslant \epsilon \leqslant \epsilon'')$$

or

$$\log \sigma = n \log \epsilon + \log A$$

11

where σ = applied stress

ε = residual strain

ε', ... assigned values of strain in the low strain regime

n = strain exponent

A = proportionality constant

(The value of n, the strain exponent, which corresponds to the slope on the log-log plot, is believed to be indicative of the strain hardening processes in the material. It should be noted that the lowest value that ε' can physically assume is zero. This case, however, corresponds to the situation where even the minimum application of load results in a finite, albeit small, residual plastic deformation.)

The curves obtained by replotting the microyield data for the different samples on logarithmic coordinates are shown in Figure 3. All of the curves appeared quite linear in the low strain regime (less than about 5×10^{-5} strain) and some showed departures from linearity at the higher strain levels. What was clearly evident, by plotting the data in this manner, was that the value of the empirically defined strain exponent was strongly affected by some of the heat treatments that were employed. The observed differences in the slopes of the various plots illustrates the limited utility of the conventionally defined microyield strength in determining long-term microcreep effects. Depending on the level of residual strain that is selected (in our arbitrary assignment) for designating the corresponding applied stress value as the microyield strength, a specific thermal treatment for a material could be (improperly) construed as being most beneficial from a performance point of view. Whereas for strain levels of 10^{-6} and less, a higher microyield value is indicated for the HIP-50 material after a 1055°C, 2-hour quick-cool plus 370°C, 24-hour thermal aging treatment (compared to the as-HIPed condition), this situation is reversed if strain levels of about 10^{-5} are considered. A similar situation is also indicated for curves (c) and (d) in Figure 3 with the cross-over possibly occurring in this case at values close to about 10^{-7} residual strain. The data clearly show that if a correlation is sought between the behaviors of

12

microyield and microcreep, it is essential to somehow factor the slope, obtained in the low strain region of microyield data (plotted on logarithmic coordinates), into such a correlation. The arbitrarily selected applied stress value corresponding to 10^{-11} strain is not, in itself, a sufficient measure of the quality of the material that results from the several selected thermal treatments.

The value of the empirically defined strain exponent did not change appreciably with the 600°C, 100-hour heat treatment of the as-received HIP-50 material. A substantial amount of strengthening, however, did result from this heat treatment over the as-received condition (which was evident in the higher applied stress values plotted in Figure 3 for equivalent amounts of residual strain). These observations were rationalized as being related to increased strengthening resulting from possible additional precipitation processes in the material which did not alter the nature of the strain hardening mechanisms. The observations made on the 600°C, 100-hour heat-treated sample, however, contrasted significantly with those made on the other two samples which were heat treated differently. In these latter two samples, clear differences were observed for the values of the strain exponent (as indicated by the different slopes). Heat treatment of both of these samples involved initial thermal exposure to temperatures considerably higher than 600°C, and this is suspected to have significantly altered the microstructure of these materials. Changes induced as a result of these treatments must, therefore, have been responsible for the changes in slopes that were observed.

A more correct interpretation of material response to applied stresses, as state earlier, in the low strain regime, requires due consideration of the strain exponent in addition to the calculated intercept of this straight line with the vertical axis at a given, very low value of residual strain, such as 10^{-10} [1]. (A strain of 10^{-10} implies a permanent uni-axial displacement of ten angstroms for a sample
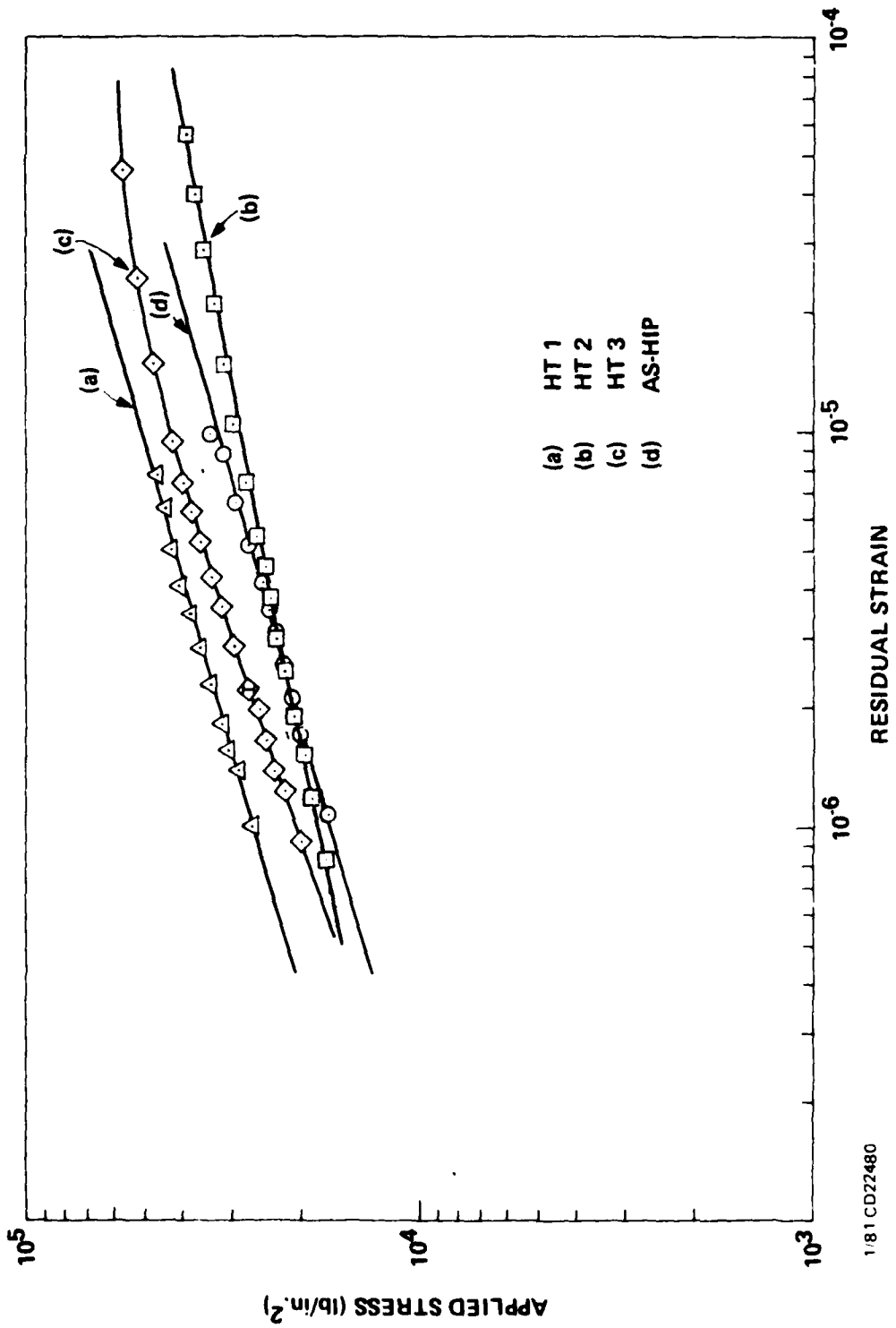
13

Figure 1. Microyield data plotted on logarithmic coordinates.

1/81 CD22480

14

10 meters long. This low value may be considered as reflecting negligible deformation.) The measured values of the slopes and the calculated 10^{-10} microyield values for the several heat treated samples are shown in Table II.

Table II. Measured values of slope n and calculated values of
microyield strength at a strain level of
10^{-10}, σ (10^{-10}).

Heat Treatment Condition	σ (10^{-10}), K lb/in.^{2}	n
As-HIP	1.3	0.28
HT1	1.9	0.28
HT2	2.8	0.20
HT3	0.9	0.34

An extension of this reasoning suggests that this calculated intercept can possibly be considered as indicative of a minimum threshold stress which is needed for initiating short-term plastic deformation, to an extent somewhat recognizable (10^{-10}) in the HIP 50 material. Of course, the validity of such a calculated value depends upon the assumption that the linear relationship observed in the 10^{-6} strain regime remains unchanged for even lower strain values (at least down to 10^{-10} strain). That different threshold values of the stress exist for each of the samples examined was suggested in the nonconverging nature of the straight lines as they approach progressively lower strain levels. According to this analysis, when the threshold value of stress is exceeded, plastic deformation occurs (which shows up as a minimum residual strain). Further short-term material response to applied stresses is thereafter controlled by a combination of yielding and strain hardening mechanisms.

4.4   Results of Microstructure Investigations

The microstructures of the HIP-50 materials after various heat
treatments were examined using both optical and transmission electron
microscopy. These studies were performed on extra samples of HIP-50
materials that were enclosed in the steel cans along with the microyield
specimens prior to the high temperature treatments discussed in an
earlier section.

4.4.1   Optical Microscopy

Samples representative of the different heat treatment conditions
were removed from the heat treated materials using a low speed diamond
saw. The samples were then mounted in a resin-containing clear-cast
material. Because the rate of wear for the clear-cast material was
expected to be higher than that of beryllium, this clear-cast material
was reinforced with fine Al_2O_3 powder to avoid uneven wear of the sample
surface during polishing. The samples were then polished using standard
procedures with diamond pastes containing progressively finer sizes of
diamond particles, but the final polishing operation was performed with
0.05-micron size Al_2O_3 particles dispersed in water. When these samples
were examined, using differential phase contrast (Nomarski) microscopy,
evidence of twinning (possibly resulting from stress-relief at the
polished surface) was observed in some of these. Figure 4 is
representative of what was observed. All of the optical observations
were made either on a Zeiss Universal microscope or on an American
Optical metallograph.

Following the suggestions of G. London of the Naval Air
Development Center, these samples were prepared again using extreme
caution to avoid introducing surface damage into the material as a
result of the handling procedure that was adopted. The as-cut surface
(following sectioning on the diamond saw) was mechanically abraded

15.63 μm

Figure 4. Nomarski view of as-polished HT-1 sample.

(polished) and then subjected to chemical dissolution of the surface
regions in KBI etching solution.* This process resulted in dissolution
of roughly 0.007 inches of material from the sample surface. At this
point it was felt that the outer damaged layers must have been removed
and the samples were again mounted in the Al_2O_3 particle-reinforced
resin-containing cast material. The samples were again polished with
the several grades of diamond pastes but this time care was taken to
apply minimum pressure during the several polishing stages. Following
this polishing sequence the samples were again examined on the
metallographs. This time, twinning associated with stress relief at the
surface was not observed, clearly supporting the view that the earlier
observed effects were mainly mechanically induced artifacts.

Because no good etchant is available for beryllium, the samples
were examined using Nomarski and polarized light techniques. The
micrographs observed in these two cases for the several samples are
shown in Figures 5 and 6. It was noted that no marked differences
existed in the polarized light micrographs which could provide insight
into the changes in microstructure. However, differences were indicated
to some extent in the Nomarski observations. The micrographs in Figure
5 suggest that there were differences in the wear-rates between the
grain boundary regions and the grain interior in the samples solution
treated at 1055°C and aged for 16 hours at 370°C. This sample also
showed a low 10^{-6} strain microyield strength and the lowest value of the
strain exponent. Relative differences in the other three samples were
not as prominent even though it appeared that the sample aged for

---

* Beryllium etching solution developed by Kawecki-Berylco Corp. KBI
etch consists of:

     500 ml H_2SO_4

     +500 ml Phosphoric Acid
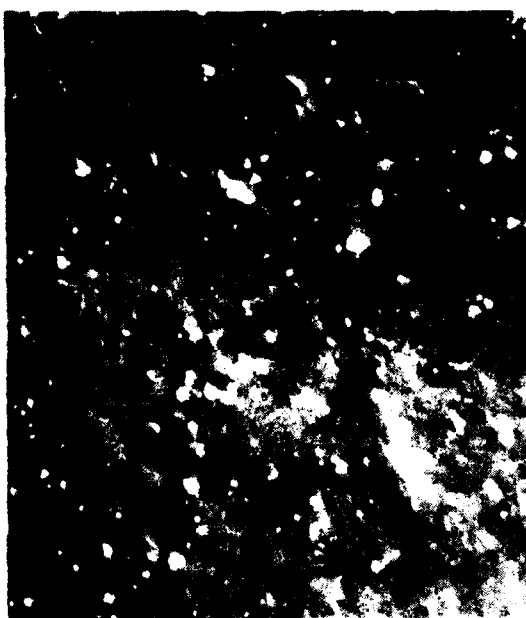
     +750 gms Chromic Acid

     +3 liters water.

(Use at 50°C)

(A) AS-HIP

15.03 μm →

(B) HT-1

(C) HT-2

1/81 C02/483

20 μm →

(D) HT-3

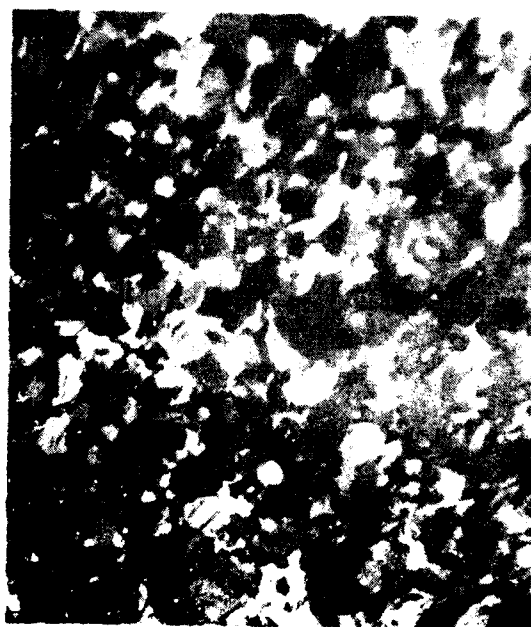Figure 8. As-produced Nominiski structure
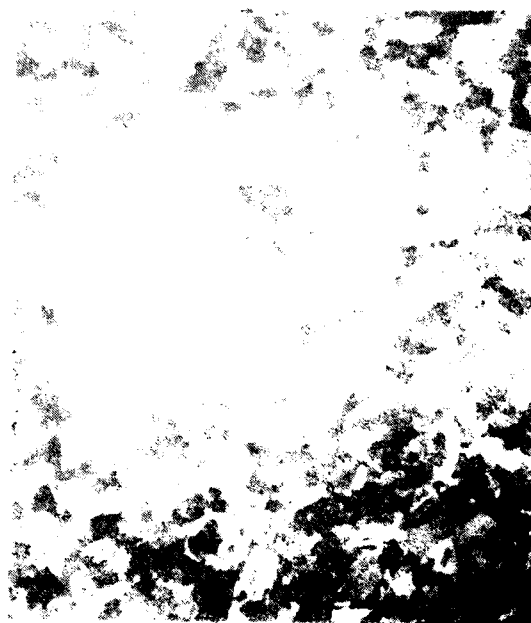
(A) AS-HIP 15.63 μm⟶

(B) HT-1 20 μm⟶

(C) HT-2 20 μm⟶

(D) HT-3 20 μm⟶

1/81 CD22484

Figure 6. As-polished polarized light micrographs.

20

100 hours at 600°C, which had earlier shown the highest microyield strength, wore away more uniformly (at the grain interiors and at the grain boundaries) than did the other two samples. This, however, could not be deduced from the micrographs with a great degree of confidence. None of the features observed at the surface could be confidently related to effects such as precipitate formation or to the presence of non-metallic inclusions, such as beryllium oxide. It was hoped that the electron microscopy technique would provide more insight into the processes that had occurred from the heat treatments that were employed.

4.4.2 Transmission Electron Microscopy

Heat-treated samples were carefully machined on a lathe into a cylinder of about 0.3-cm diameter and 1-cm length. The machined cylinders were then sliced up into 10-to-12-mils-thick discs using a low speed diamond saw. The discs were then chemically thinned down to 4-to-5 mils thickness with KBI solution. This thickness was further reduced to about 3 to 4 mils by a very gentle, low stress, lapping operation using a suspension of fine (0.3 micron) Al_2O_3 powder. The lapping operation was designed to introduce minimal surface damage while assuring the production of a reasonably well-polished surface from the matte finish that resulted after immersion in KBI solution.

For electron microscopic observation it was important to reduce the thickness considerably more than was achieved by the steps outlined above. Further thinning was accomplished using a commercial Fichione jet electrolytic polishing unit. The electrolyte impacted the flat surfaces of the discs on both sides, roughly a circular area 2mm in diameter, until such time that a hole was punctured through the specimen. At this point the unit shut off automatically through a photoelectric cell sensing a beam shining through the punctured hole. The electrolyte consisted of a mixture of 150 gms chromium trioxide, 750 ml acetic acid, and 30 ml of distilled water. Mixing was accomplished by heating the mixture to about 65°C for 1 hour to allow the chromium trioxide to go into solution. During jet-thinning of the

21

samples, the electrolyte was maintained at near-room temperature. The unit was operated at 50 volts and 25 mamp.

Electron microscopic examination of the as-received material was done earlier at the National Bureau of Standards (NBS). This was discussed in the last reporting period [4]. Similar examination of the heat-treated material during this work, on the other hand, was performed at a local facility. This change, however, required some initial development activity regarding the use of an alternate electrolyte, other than the perchloric based solution used earlier at NBS. Because the perchloric solution is quite explosive if not handled with extreme care, appropriate conditions were investigated and developed for jet-thinning of beryllium with the chromic-acetic solution described above.

Many of the micro-photographs that were obtained on the several heat treated samples, at a variety of magnifications, are shown in Figure 7. The differences indicated between the differently heat-treated specimens appeared to be primarily related to phase precipitation and segregation. The following observations were made from the data that were collected.

(1) As reported earlier for the as-HIPed material[4], these heat-treated samples also did not show significant BeO agglomerations. In instances where "small particle colonies" were observed, the particles could not be conclusively identified as BeO from the diffraction data.

(2) Diffraction data, in general, were hard to obtain. Areas that contained a fair amount of precipitates either yielded only a very small number (2 to 3) of diffraction spots (which could be indexed for Be and BeO) or did not produce any pattern at all. In some cases very diffuse patterns were obtained.
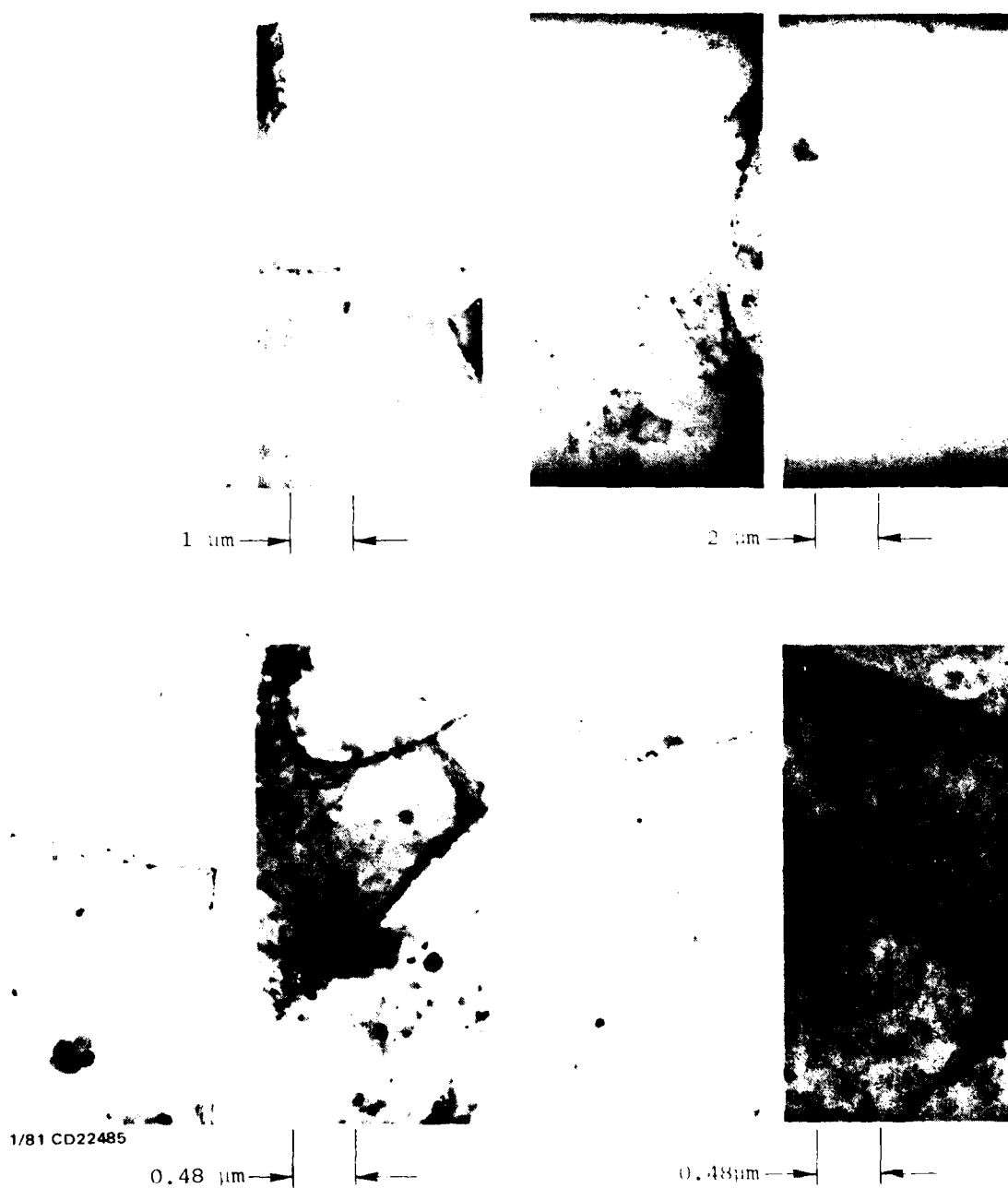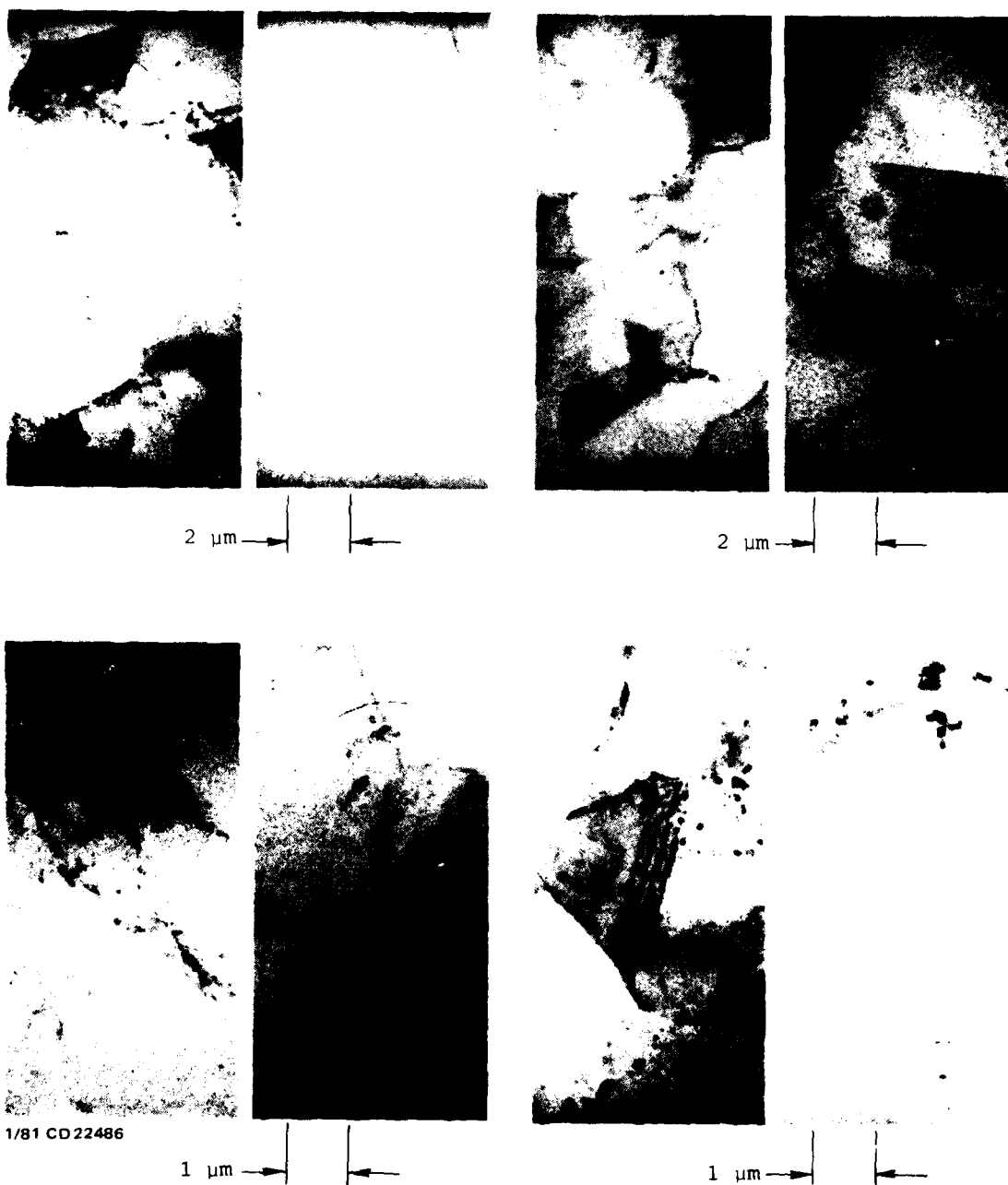
22

1/81 CD22485

Figure 7a. Electron micrographs obtained on heat treated HIP-50 materials (HT-1).

23

1/81 CD 22486

Figure 7a.   Electron micrographs obtained on heat treated
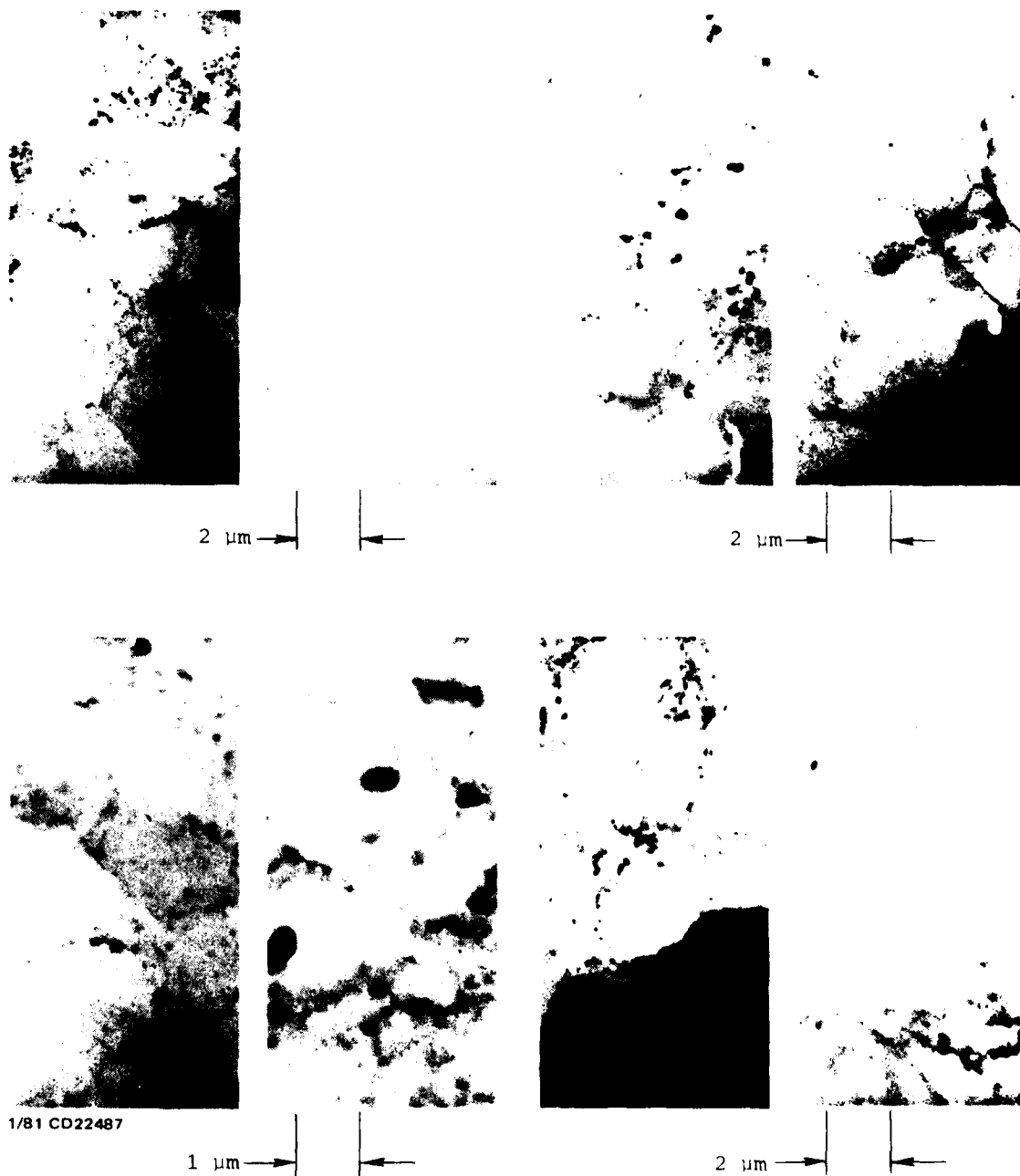HIP-50 materials (HT-1) (Continued).

24

1/81 CD22487

2 µm

2 µm

1 µm

2 µm

Figure 7b.   Electron micrographs obtained on heat treated
HIP-50 materials (HT-2).

1 μm →   ← ―   0.62 μm→   ← ―

1/81 CD22488

1 μm →   ← ―   0.48 μm→   ← ―
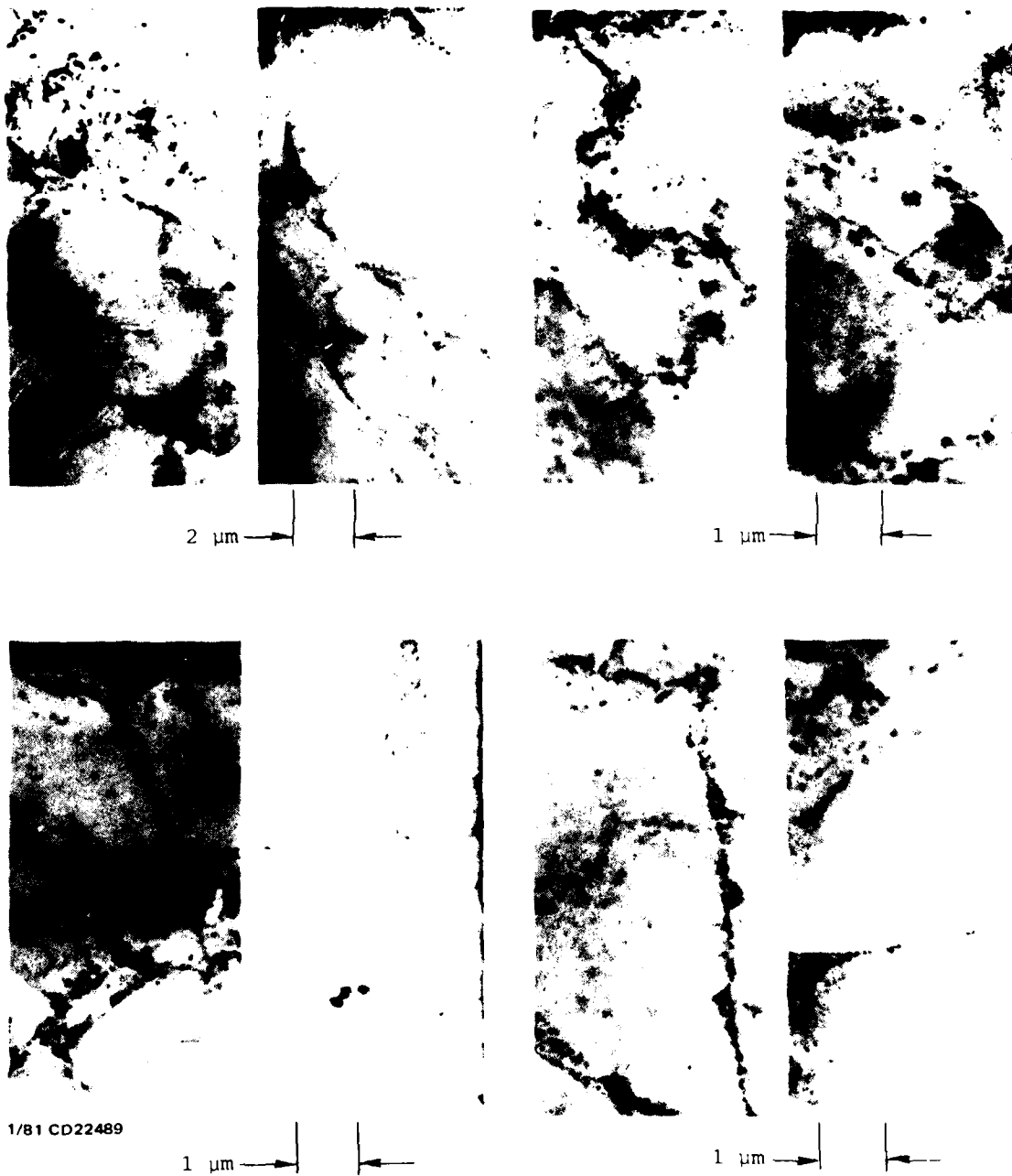
Figure 7b.   Electron micrographs obtained on heat treated
             HIP-50 materials (HT-2) (Continued).

26

Figure 7c. Electron micrographs obtained on heat treated HIP-50 materials (HT-3).

2 μm ⟶   ⟵   0.71 μm ⟶   ⟵

1/81 CD22490
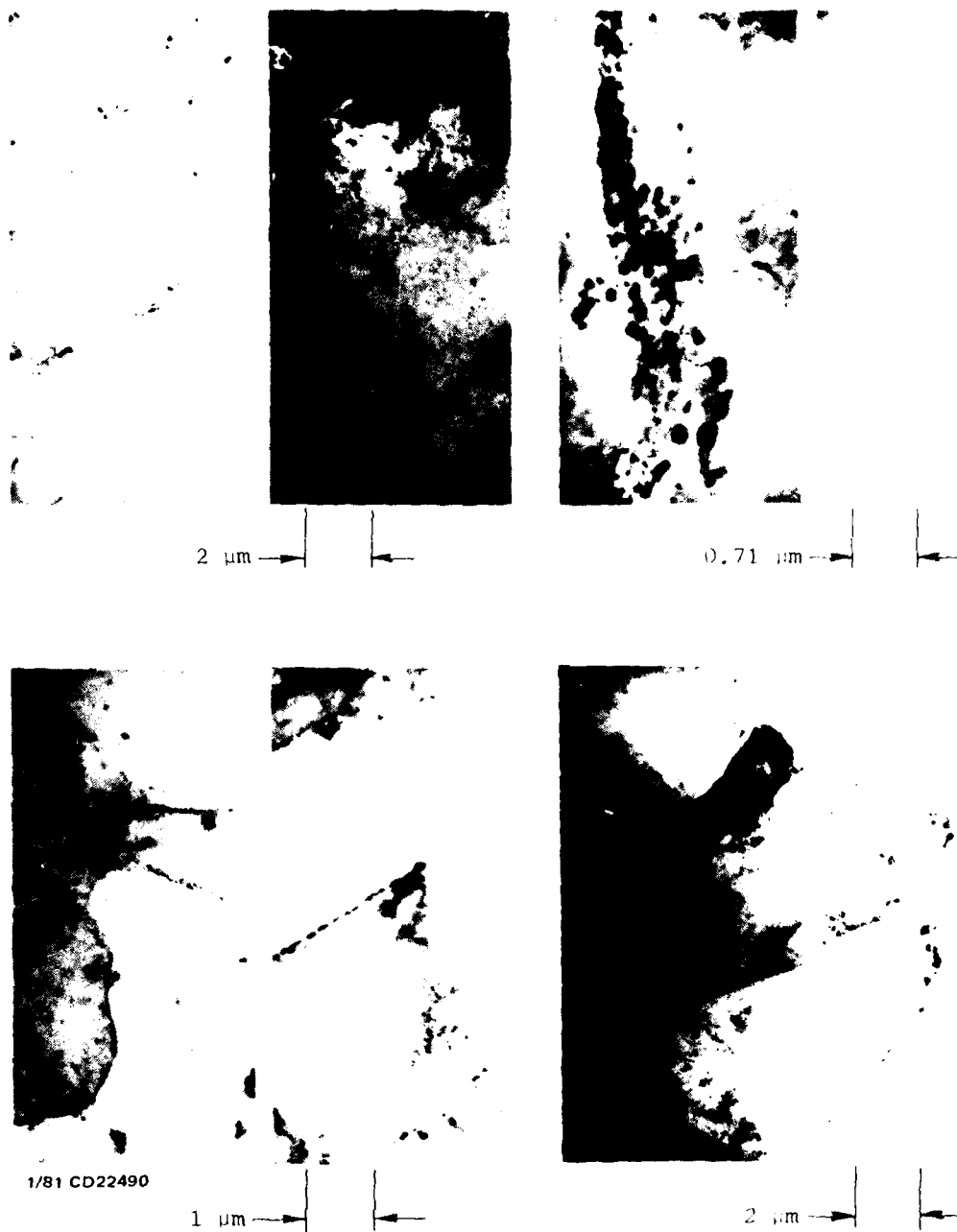
1 μm ⟶   ⟵   2 μm ⟶   ⟵

Figure 7c. Electron micrographs obtained on heat treated
            HIP-50 materials (HT-3) (Continued).

28

3) The effect of heat treatment HT1 was to produce a very slight precipitation mainly at the grain boundaries. A few boundaries also appeared reasonably clear of precipitates. Most of the grain interiors also appeared fairly precipitate-free. This may indicate why no apparent change was observed in the strain hardening mechanism (as indicated by the strain exponent) in the material from this treatment. Since strain hardening is a bulk (grain interior) effect, one can expect very little change in the strain exponent if there is no appreciable change in the microstructure. The increased amount of strengthening (over the as-HIPed state), as observed at the 10^{-6} and higher strain levels, may have actually resulted from additional strengthening of the grain boundary regions by the newly formed precipitates.

(4) Precipitation was found to have occurred more extensively in the HT2 heat-treated specimen as compared to the other materials. Unlike the other samples, however, this one showed substantial precipitation at the boundaries as well as in the grain interiors. An overall preference for the grain boundary regions was, nevertheless, indicated. (These observations were somewhat unexpected in that very little precipitation was intuitively expected from a 370°C exposure following a high temperature solution treatment at 1055°C.) The reasonably large amount of precipitation within the grains might have been responsible for the reduced level of strain hardening (as indicated by the strain exponent) in this material. The highest value calculated for σ (10^{-10}) in this instance and the indicated differences in removal rates for the boundary versus the interior regions, however, cannot be explained on the basis of these observations. It was noted that no apparent change in grain size resulted from this heat treatment.

29

(5) A larger amount of grain boundary precipitation (more so than was found for the HT1 sample) was found in the sample subjected to the HT3 treatment. As with the HT1 sample, the grain interiors of the HT3 sample also appeared relatively clear of precipitates, therefore accounting for the retention of a high value of the strain exponent. It was, however, not clear from these studies as to why the measured strain exponent value for the HT3 sample was higher than those measured for the as-HIPed and HT1 heat-treated conditions.

4.5   Microcreep Analytical Studies

4.5.1   Review of Past Activities

The purpose of the analytical studies has been to apply the creep laws to gyro design, to try and give direction to the microcreep experiments from a design viewpoint, and to support the experimental activities with finite element analysis.

Previous reports have shown that analysis of instrument trends due to microcreep, using available finite element codes, is feasible. However, unless the creep characteristics of beryllium and other instrument materials is understood, this conclusion will be suspect. To date, sufficient data and understanding have not been attained.

Initially, inertial instruments were designed using the microyield strength of beryllium as a design limit. Experiments over the past 10 to 15 years on test specimens have shown microcreep to occur at stress levels far below the microyield strength. This has resulted in a question of what values to use as design limits, especially for future generations of inertial instruments. Although knowledge of microcreep is still vague, the ability to accurately compute elastic and plastic stresses has grown enormously in the past 10 to 15 years. This growth has occurred due to the continual improvement of computers and

numerical methods (i.e. finite element method). Therefore, accurate
knowledge of the constitutive equations of materials such as beryllium
could lead to the very accurate design predictions and design
improvements.

4.5.2   Analysis of Test Specimens

In support of the design of a tension microcreep experiment at
CSDL, analysis of stress distributions within test specimens has been
performed.

4.5.2.1 Test Specimen Description and Model

Since the capacitance probe measurement technique was selected
for measuring creep movement, a method of attaching them to the specimen
must be selected. A test specimen using axisymmetric ribs was initially
proposed, as shown in Figure 8. An axisymmetric model of half of the
specimen using 8-node quadratic bricks was constructed. This model
consisted of 69 elements and 250 nodes as shown in Figure 9. The area
under the rib was modeled in finer detail than the simple circular
sections away from the rib.

4.5.2.2 Analysis - Axisymmetric Design

The loading condition was applied as a uniform negative pressure
along the surface of the five last elements in the one direction.
Symmetry conditions were applied at the mid-plane. A nominal load of
100 pounds was applied to the specimen. A contour plot of the Mises
stresses is shown in Figure 10. It is observed that there are two areas
of disturbance. The first is produced by the end grips and the second
by the support ribs for the capacitance plates. Since the end grip
disturbance dies out before the test section, it is of no consequence.
However, the supporting ribs for the capacitor plates do influence the
stress field in the test section. An enlargement of the stress contours
in this area is shown in Figure 11. It is observed that the stress
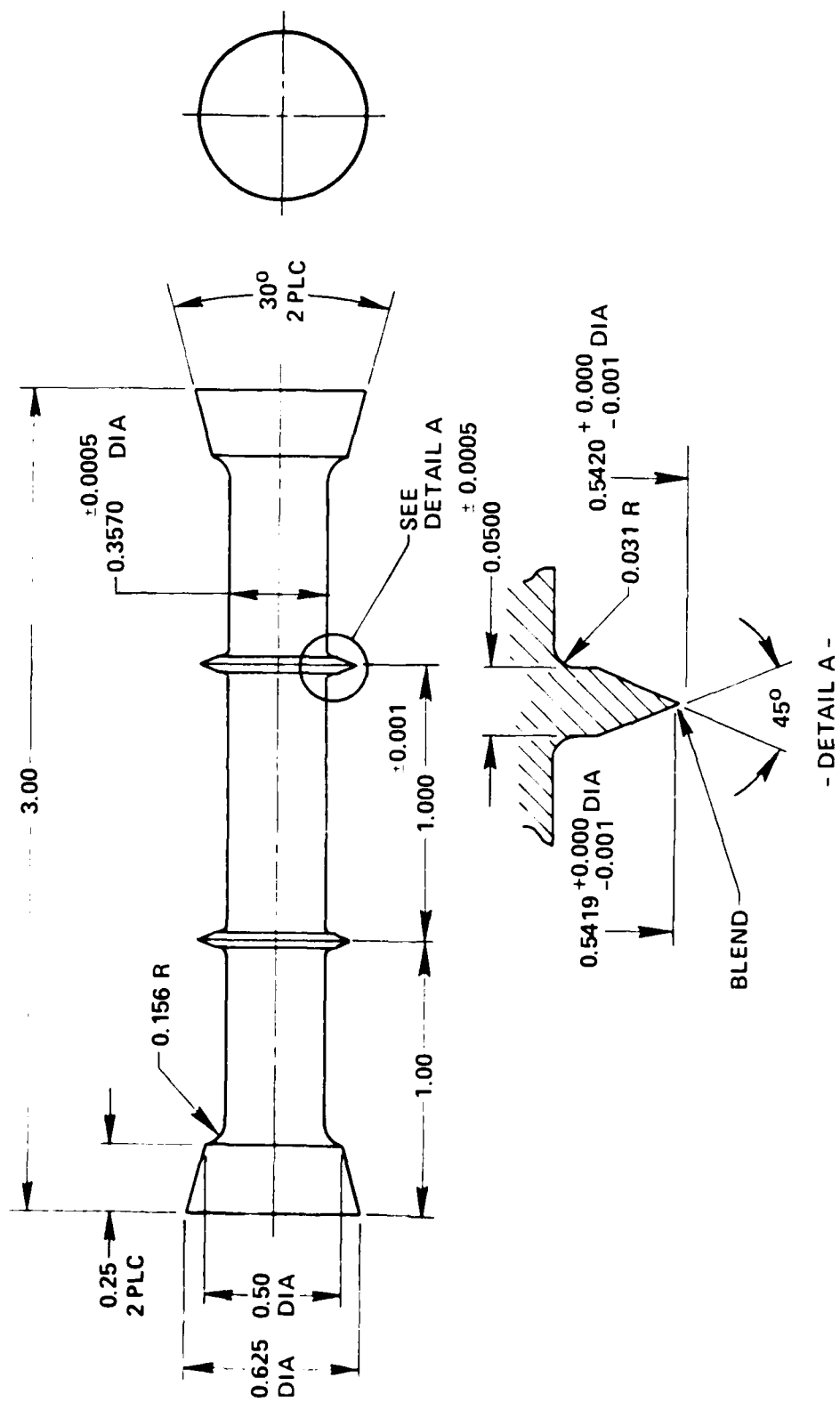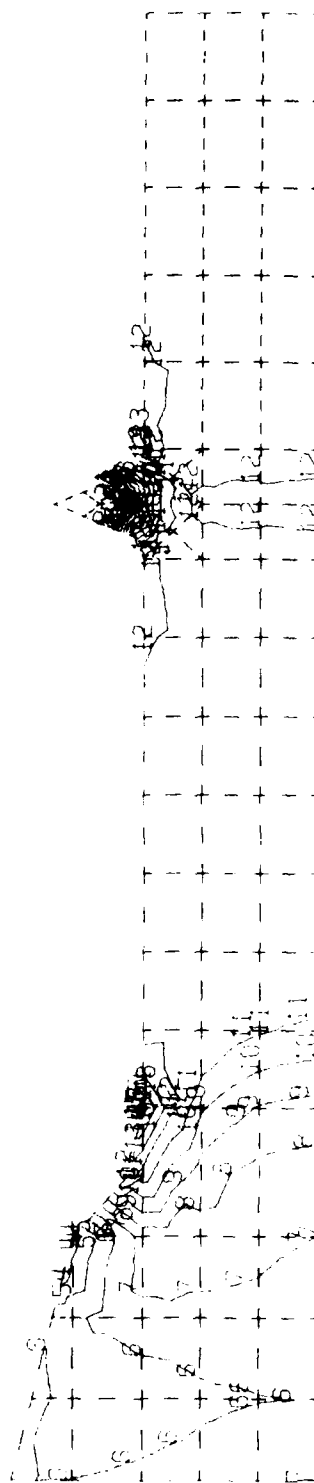
31

Figure 8. Proposed test specimen with axisymmetric ribs.

Figure 9. Axisymmetric finite element model.

2/81CD22643

33

CONTOURS
1 — 3.75 E1
2 — 1.26 E2
3 — 2.14 E2
4 — 3.02 E2
5 — 3.91 E2
6 — 4.79 E2
7 — 5.67 E2
8 — 6.55 E2
9 — 7.44 E2
10 — 8.32 E2
11 — 9.20 E2
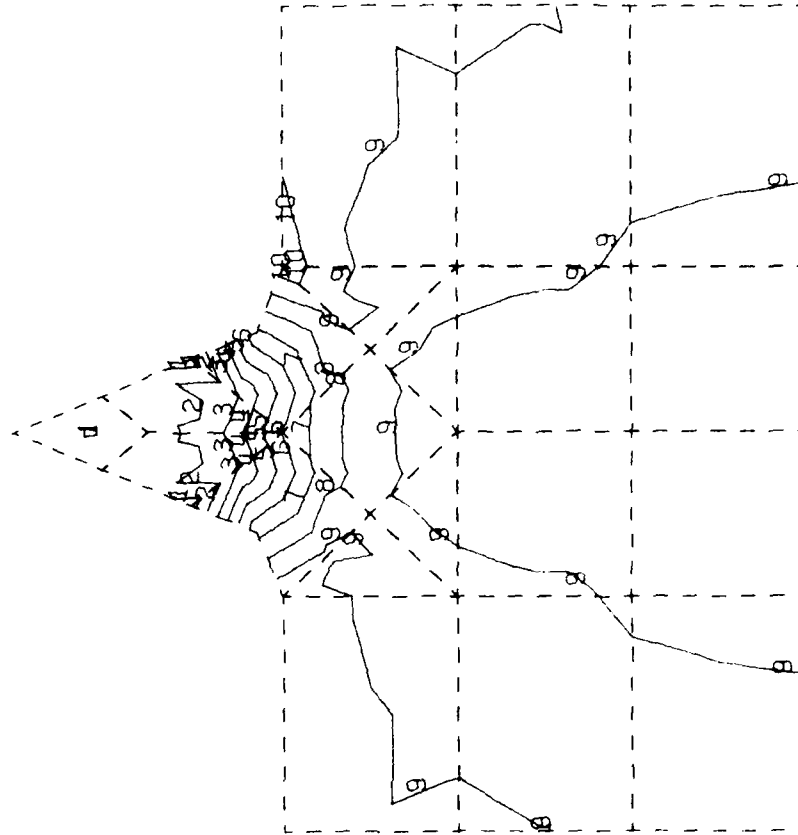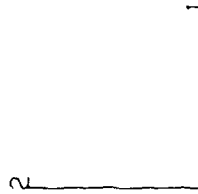12 — 1.01 E3
13 — 1.10 E3
14 — 1.19 E3
15 — 1.27 E3

Figure 16. Deflection of the ... field stress, axisymmetric model.

2/81 CD22644

CONTOURS

1 = 5.12 E1
2 = 1.67 E2
3 = 2.82 E2
4 = 3.98 E2
5 = 5.14 E2
6 = 6.29 E2
7 = 7.45 E2
8 = 8.61 E2
9 = 9.76 E2
10 = 1.09 E3

Figure 11. Beryllium specimen Mises stress, support rib.

2/81 CD22645

levels decrease as they approach the rib, reach a minimum before the center of the rib, increase to a peak at the center of the rib, and then decrease and increase symmetrically on the other side. A plot showing the elastic displacement of the test specimen is shown in Figure 12.

In order to better observe the axial variation of the stress fields, the axial stress (one direction) at the gaussian integration points of the elements at a fixed radial distance were plotted versus axial distance. Since only the disturbance produced by the capacitor ribs are of interest, the plots originate .4 inches before the center of the rib which occurs at 1.0 inch. Figures 13, 14 and 15 show these plots starting at a radius of .007 inches. Figure 13 shows the axial variation at radii of .007, .030 and .053 inches. Figure 14 repeats the .053-inch radius and also plots .066 inch. Figure 15 shows plots at radii of .066, .089 and .112 inches. The first four points have similar trends reaching minimum and maximum at the same points. The last two radial locations start to deviate since they are approaching the region directly under the capacitor rib. Only every third data point is plotted to avoid confusion, and points are linearly connected. It is of interest to note that the disturbance propagates more than half the distance to the specimen's midplane although the level of disturbance is almost always less that 5 percent.

In order to verify the numerical accuracy of this solution the grid size was halved everywhere except in the rib itself where the elements are of the same dimensional size as the new elements in this refined grid. The refined model is shown in Figure 16. Figures 17 and 18 give contour plots of Mises stresses in the specimen comparable to Figures 10 and 11. Although the contour levels plotted are different, inspection of the results shows excellent agreement between the original and refined mesh.
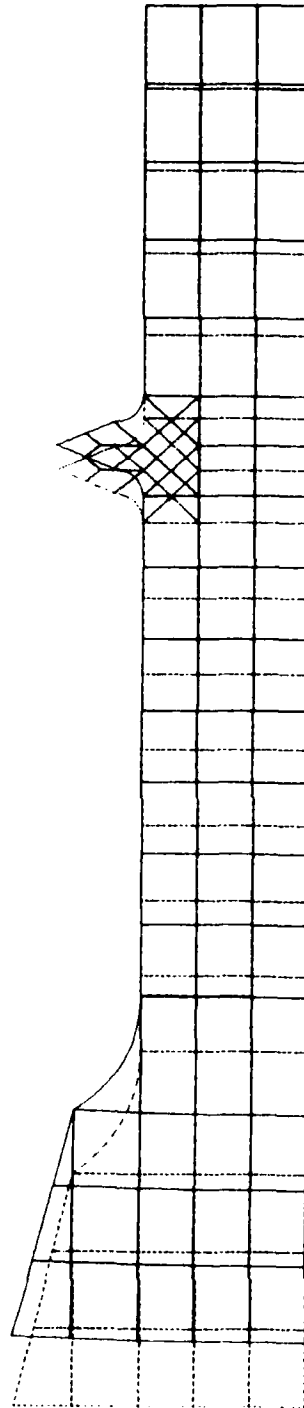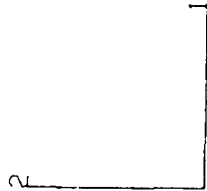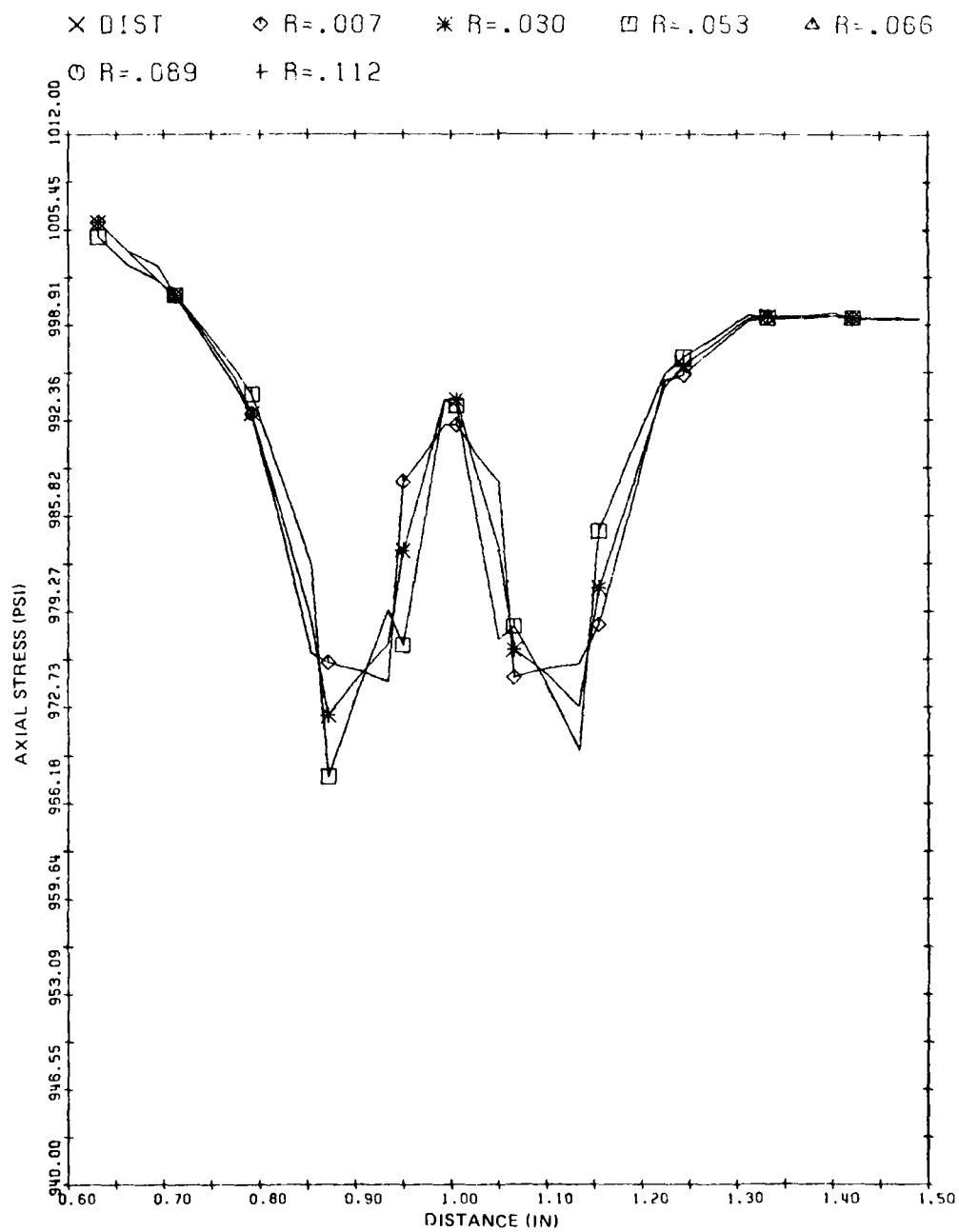
Figure 12. Beryllium specimen displacement.

2/81 CD22635

37

Figure 13. Axial stress plot, axisymmetric model, core.

2/81 CD22636

38

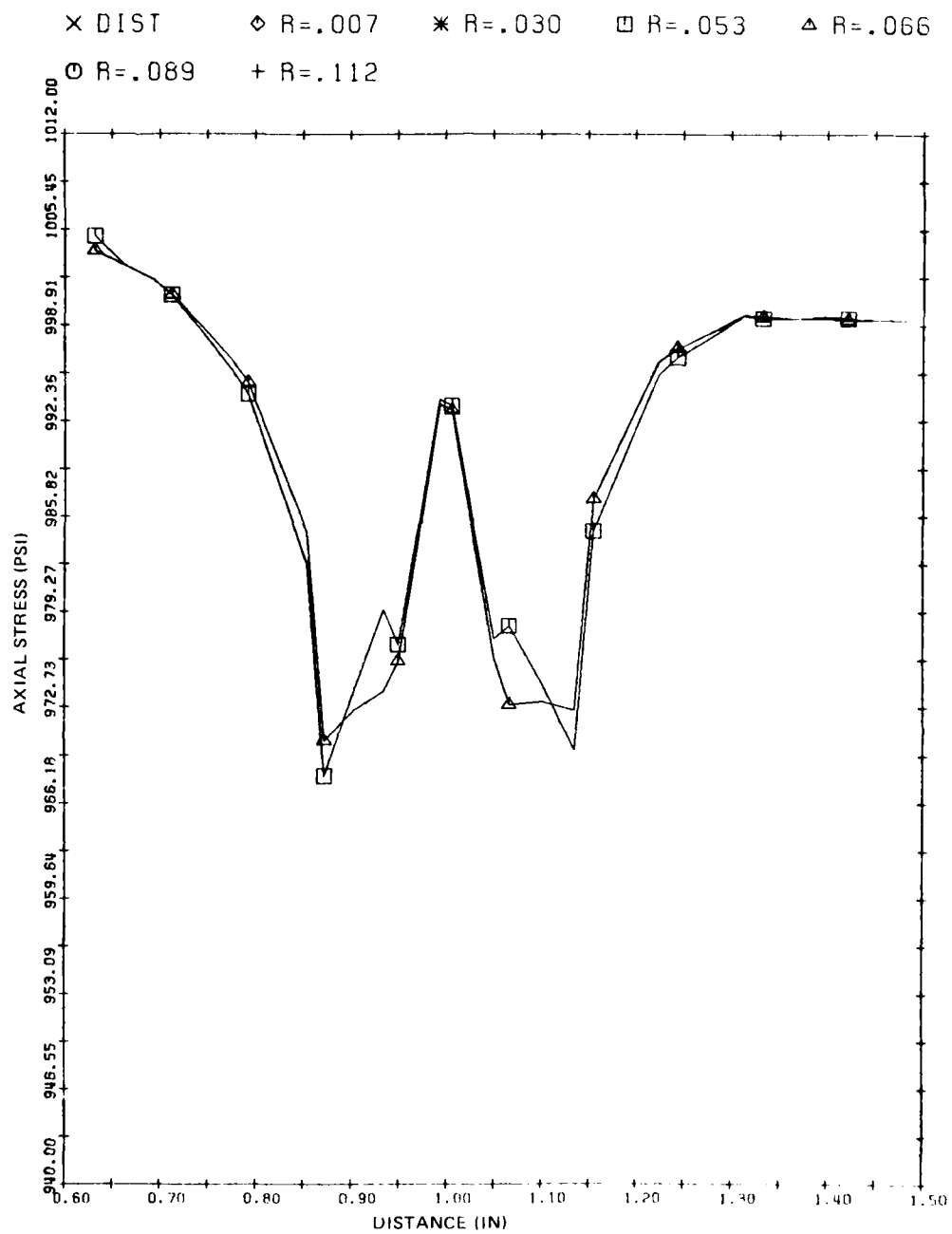X DIST   ◊ R=.007   ✳ R=.030   ⊡ R=.053   △ R=.066
⊙ R=.089   + R=.112

2/81 CD22637
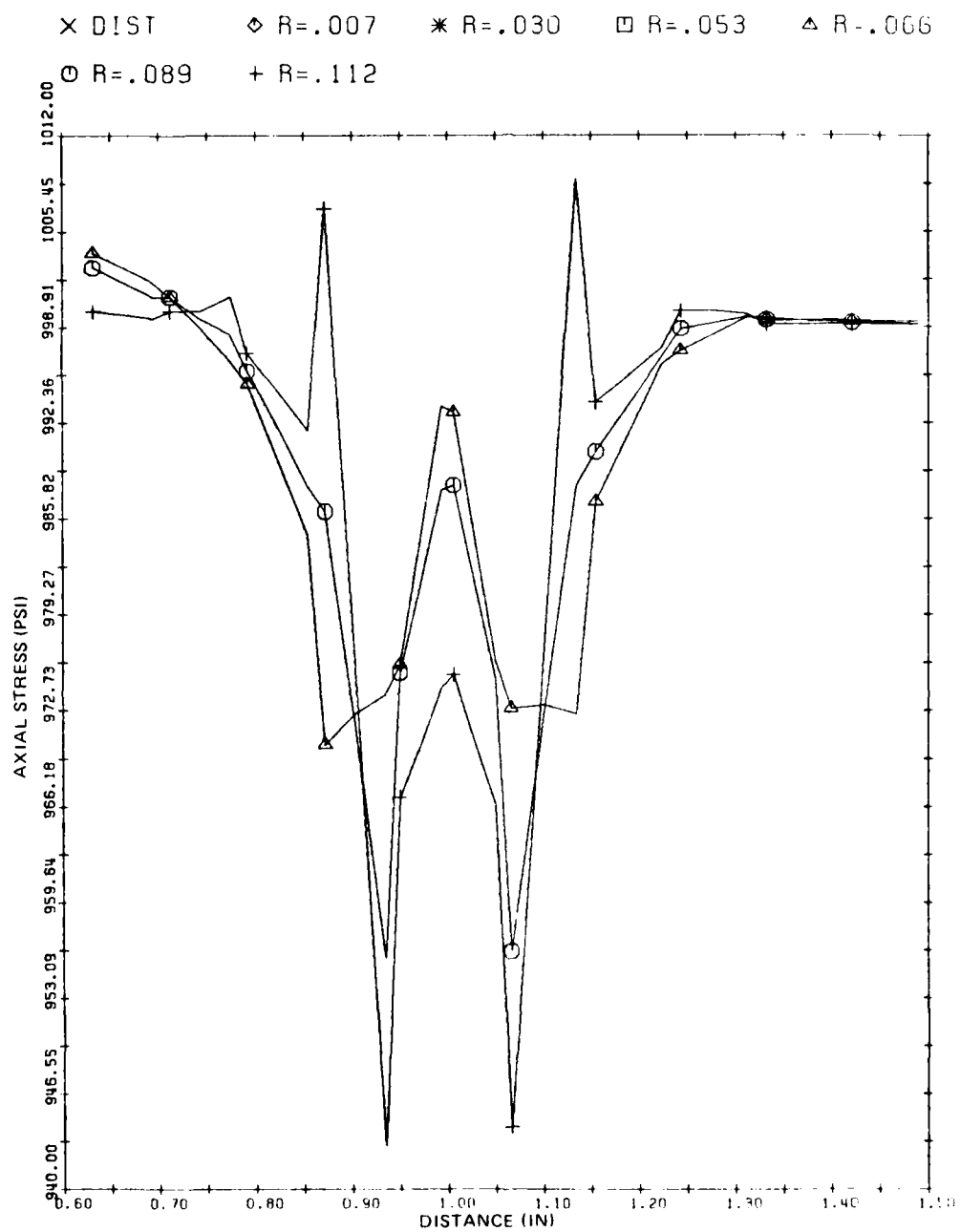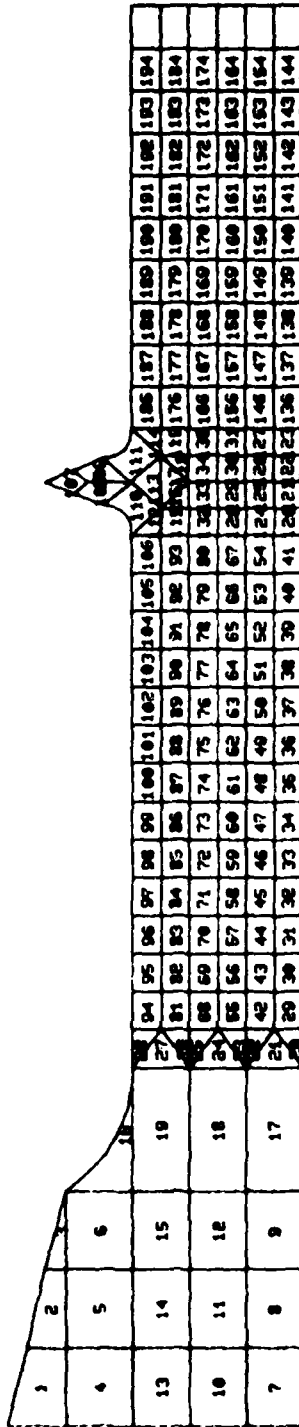
Figure 14. Axial stress plot, axisymmetric model, mid-radius.

39

Figure 15. Axial stress plot, axisymmetric model, outer shell.
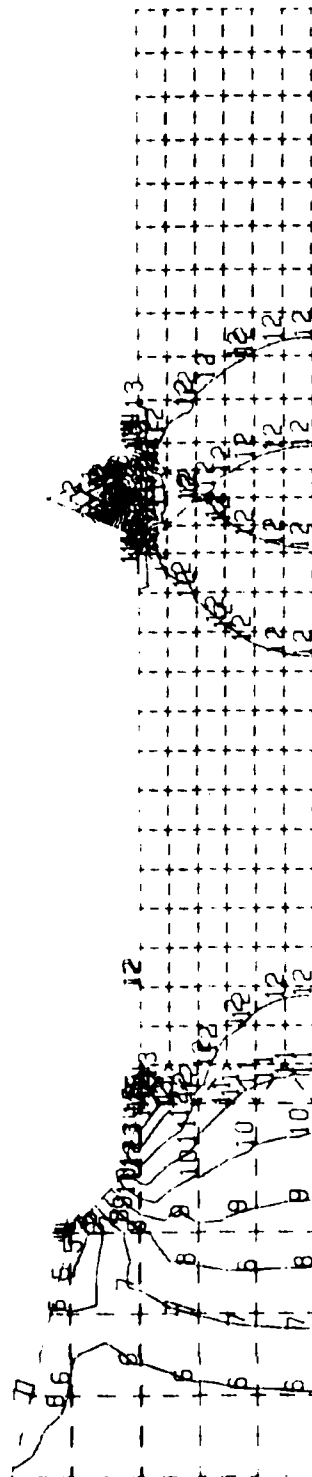
2/81 CD22638

40

MESH HAS 646 NODES AND 195 ELEMENTS OF TYPE 28
FILE : CSM4532.TEST.DATA
TITLE :
SCALE : 0.98E+01 HARDCOPY SCALE = 0.58E+01
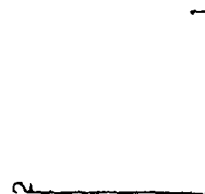DATE : 11/21/80 TIME : 13:14:23 AREA = 0.390E+00

CONTOURS
1 = -1.20 E2
2 = -1.94 E1
3 = 8.08 E1
4 = 1.81 E2
5 = 2.81 E2
6 = 3.81 E2
7 = 4.82 E2
8 = 5.82 E2
9 = 6.82 E2
10 = 7.62 E2
11 = 8.62 E2
12 = 9.82 E2
13 = 1.08 E3
14 = 1.18 E3
15 = 1.28 E3

Figure 1. Beryllium chamber, Mises stress, refined axisymmetric model

2 81 CD22640

42

CONTOURS
1 = -1.01 E2
2 = 3.54 E1
3 = 1.72 E2
4 = 3.09 E2
5 = 4.46 E2
6 = 5.82 E2
7 = 7.19 E2
8 = 8.56 E2
9 = 9.93 E2
10 = 1.13 E3

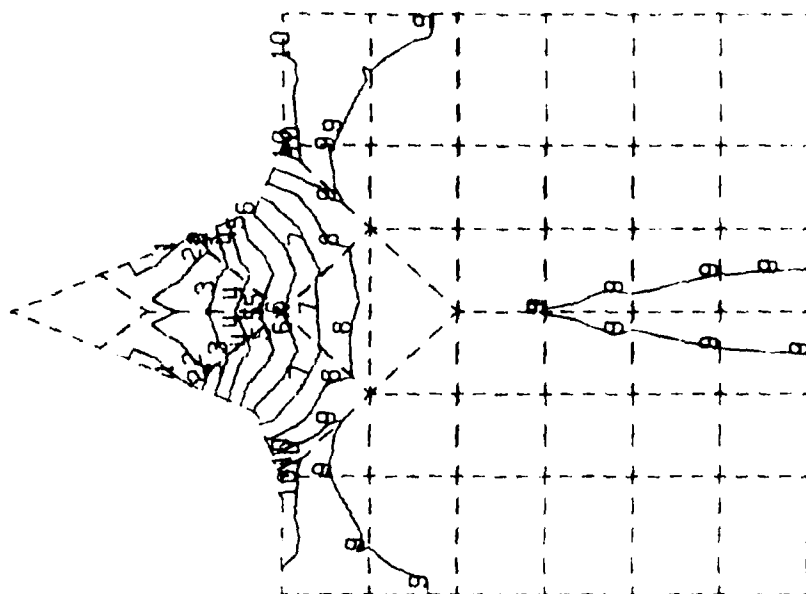Figure 16. Beryllium specimen axial stress contours by computer code.

2 81 CD22641

4.5.2.3 Analysis - Modified Design

In order to reduce the effect of the end disturbances, a modified design was proposed which would support each capacitor plate assembly on three equally-spaced lugs rather than a full circumferential rim. A layout of this design is shown in Figure 19. In order to analyze the stress distribution within the specimen a three-dimensional model is now required. However, since symmetry occurs every 60° the model was limited to a 60° segment with symmetry boundary conditions at the 0° and 60° plane. A 121-element, 608-node model consisting of 20-node bricks was constructed as shown in Figure 13. The grip portion was not considered since it was shown previously not to affect the test section. Uniform tensile loading was considered with symmetry applied at the mid-plane and also at the 0° and 60° planes as discussed above.

Axial contour plots of Mises stresses at location 5°, 15° and 50° away from the center of the lug are shown in Figures 21, 22 and 23. The contours for the 5° plot which cuts through the lug are similar to those produced by the axisymmetric model. At 15° (Figure 22), just outside the lug, the disturbance is greatly reduced. In the 50° section, as seen in Figure 23, the disturbances are less than 1 percent. A circumferential contour plot taken through the cross section is shown in Figure 24. The rapid decrease in disturbances away from the lug support is again apparent. Figures 25 to 33 plot axial stress vs. axial distance at the same radial locations plotted for the axisymmetric specimens (Figures 13-15). Figures 25-27 show plots 5° away from the lug center, Figures 28-30 show plots 15° away, and Figures 31-33 show plots 50° away. The plots 5° away show stress variations less than axisymmetric results except for the peak values that occur for the plots

44

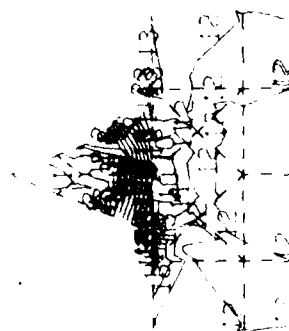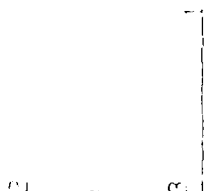20°

20°

0.542
DIA

0.357
DIA

0.031 R
6 PLC

REPRESENTS 0.031 R
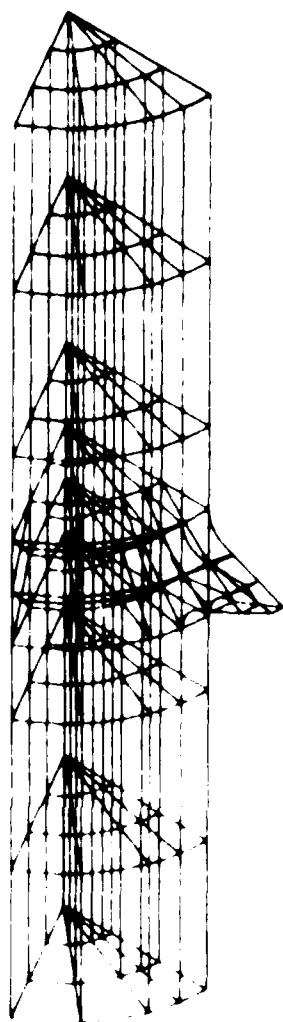
CONTOURS
1 - 6.37 E1
2 - 1.48 E2
3 - 2.32 E2
4 - 3.16 E2
5 - 4.00 E2
6 - 4.84 E2
7 - 5.68 E2
8 - 6.52 E2
9 - 7.36 E2
10 - 8.20 E2
11 - 9.04 E2
12 - 9.88 E2
13 - 1.07 E3
14 - 1.16 E3
15 - 1.24 E3

Figure 21. Beryllium specimen Mises stress -5 degrees.

2 81 CD22621

47

CONTOURS
1   9.22 E2
2   9.29 E2
3   9.36 E2
4   9.43 E2
5   9.50 E2
6   9.57 E2
7   9.64 E2
8   9.71 E2
9   9.78 E2
10 9.85 E2
11 9.92 E2
12 9.99 E2
13 1.01 E3
14 1.01 E3
15 1.02 E3

Coupling specimen Mises stress - 75 degrees.

2 81 CD22623

44
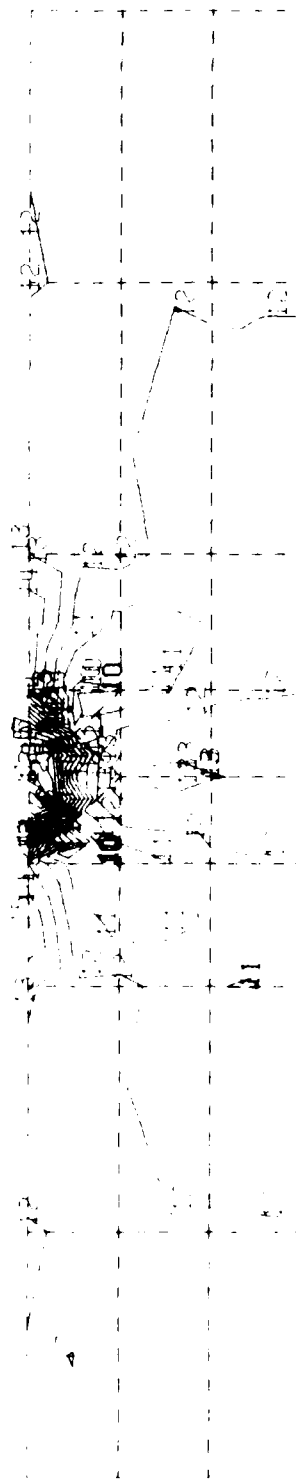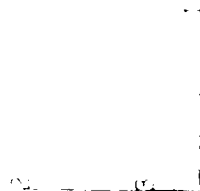
CONTOURS

1 = 9.33 E2
2 = 9.93 E2
3 = 9.94 E2
4 = 9.95 E2
5 = 9.96 E2
6 = 9.97 E2
7 = 9.97 E2
8 = 9.98 E2
9 = 9.99 E2
10 = 10.00 E2
11 = 1.00 E3
12 = 1.00 E3
13 = 1.00 E3
14 = 1.00 E3
15 = 1.00 E3
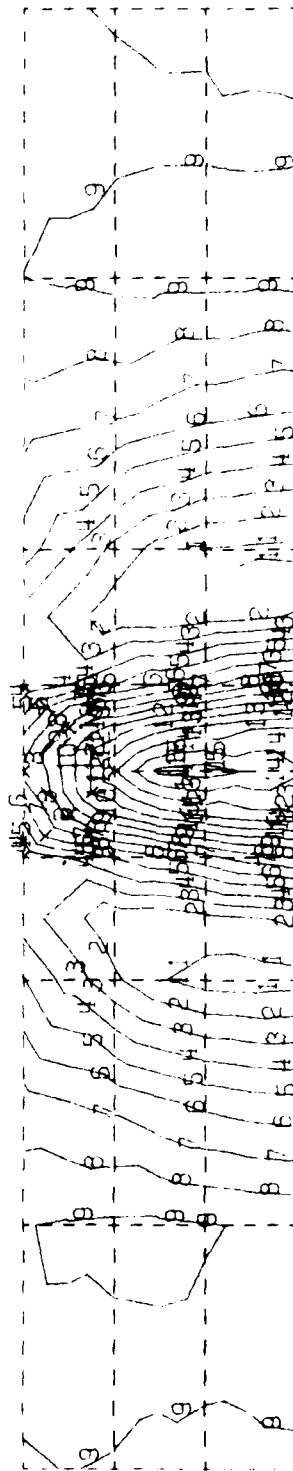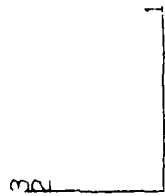
Figure 23. Beryllium specimen Mises stress - 50 degrees.

2/81 CD22624

49

Figure 24. Beryllium Specimen, Shear Stress — Cross Sectional View.

CONTOURS
1 = 5.08 E1
2 = 1.20 E2
3 = 1.89 E2
4 = 2.58 E2
5 = 3.27 E2
6 = 3.96 E2
7 = 4.65 E2
8 = 5.34 E2
9 = 6.04 E2
10 = 6.73 E2
11 = 7.42 E2
12 = 8.11 E2
13 = 8.80 E2
14 = 9.49 E2
15 = 1.02 E3
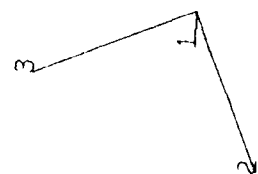
2/81 CD22622
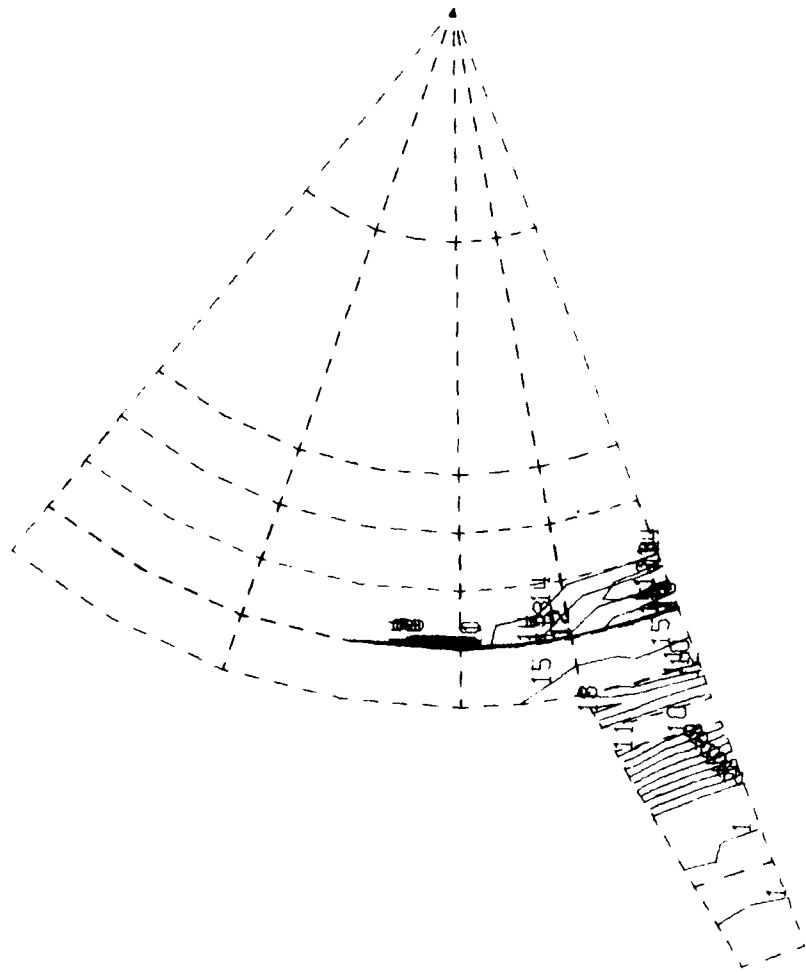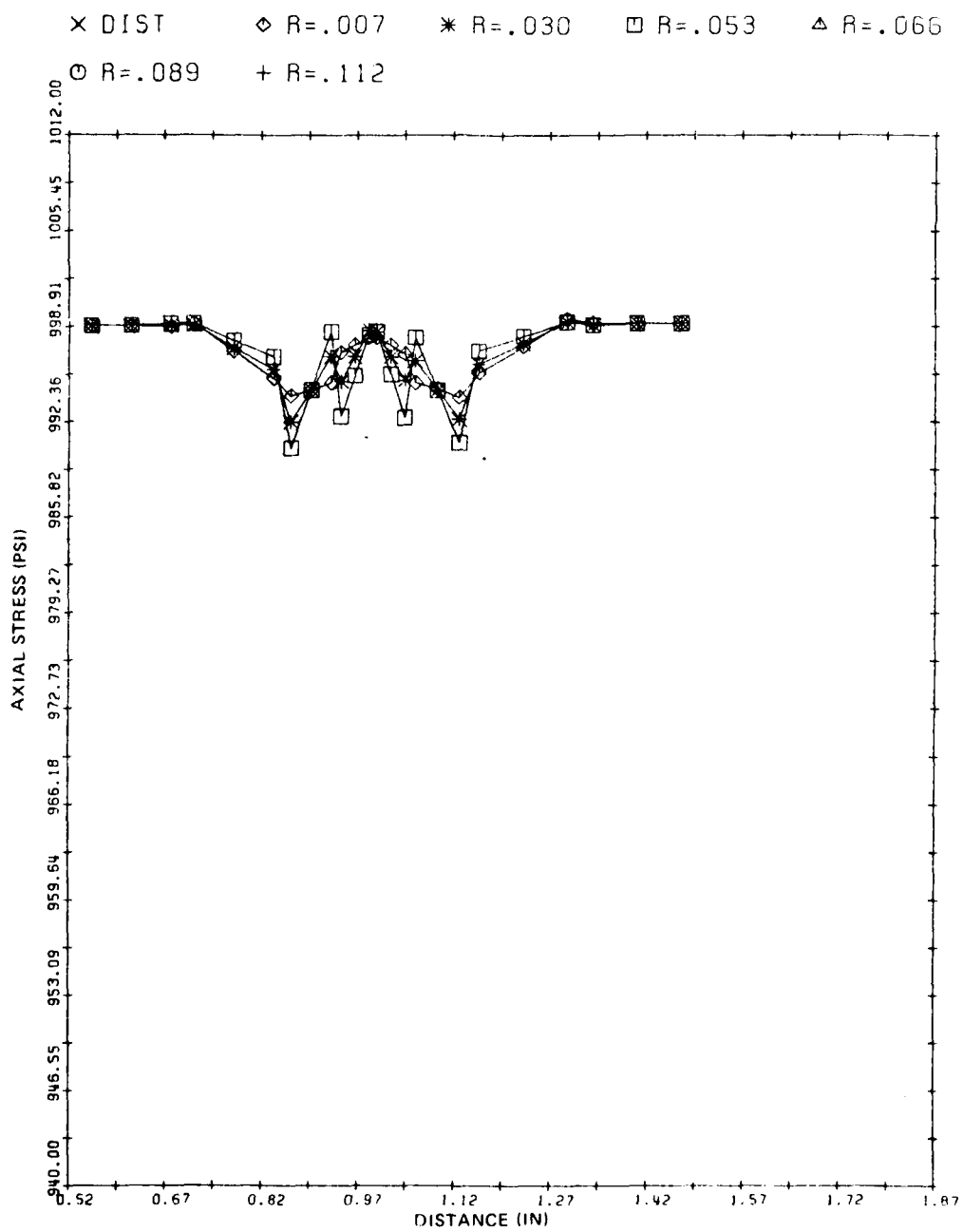
Figure 25. Axial stress plot at 5 degrees, core.

51
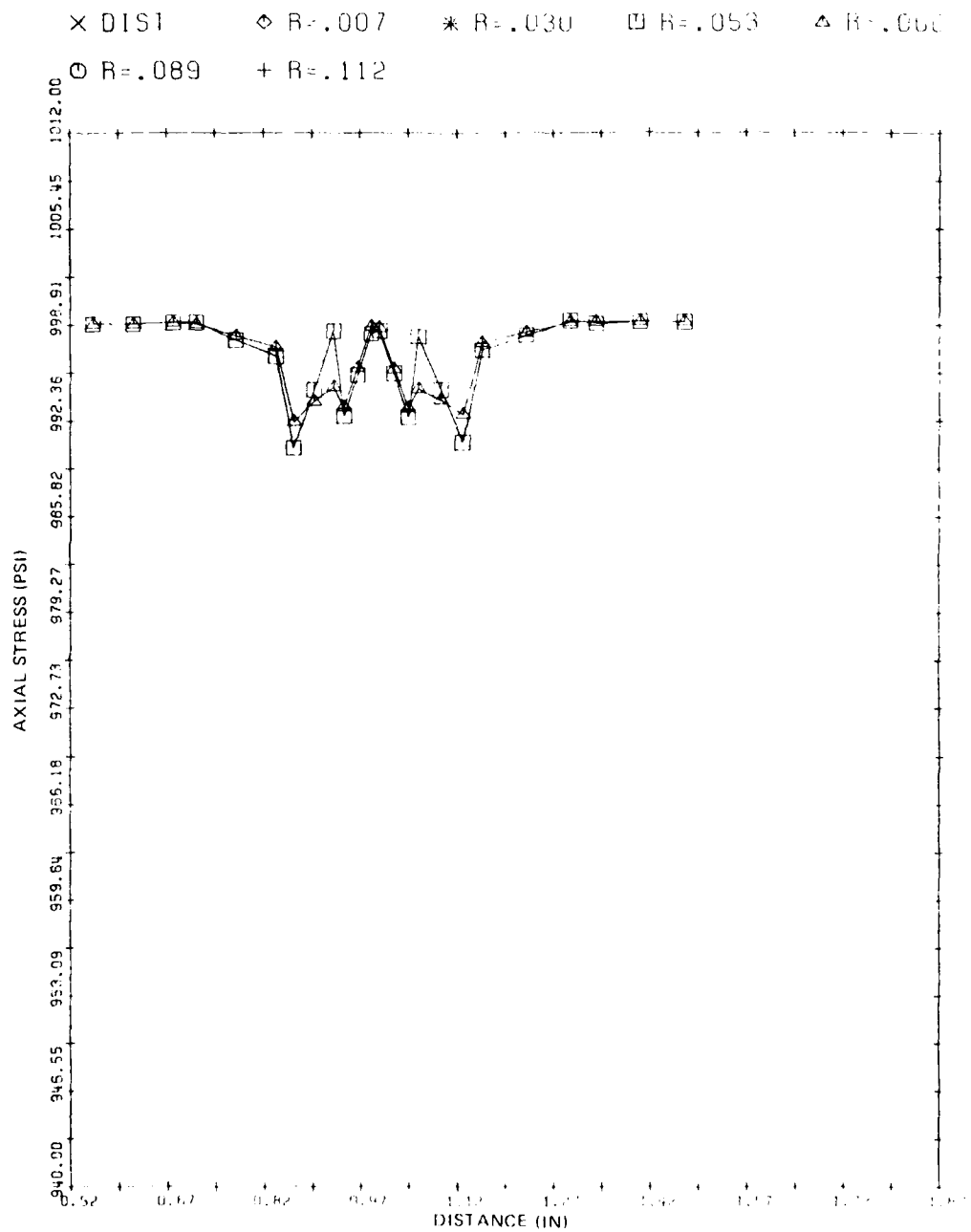
Figure 26. Axial stress plot at 5 degrees, mid-radius.

2/81 CO22626
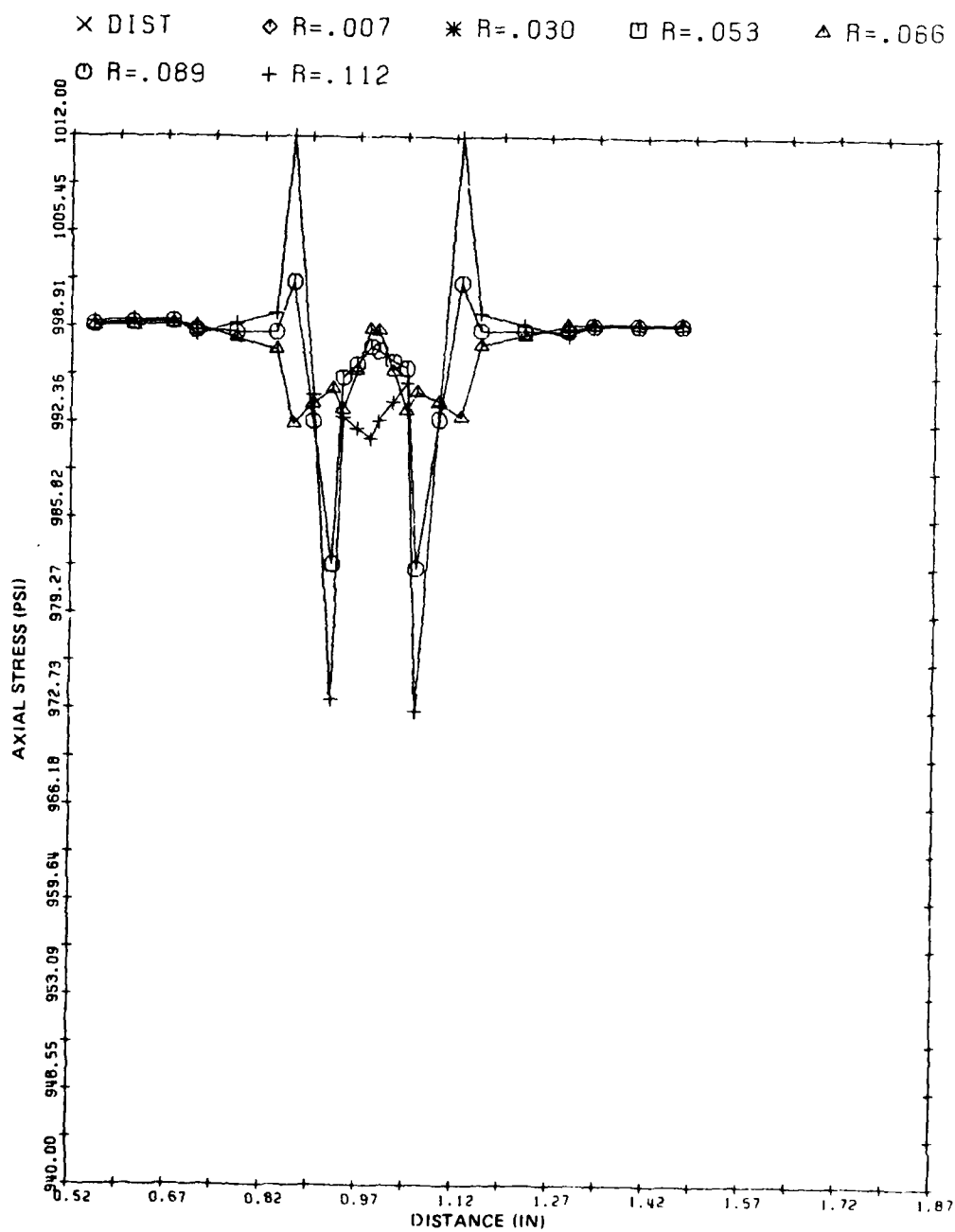
Figure 27. Axial stress plot at 5 degrees, outer shell.

53
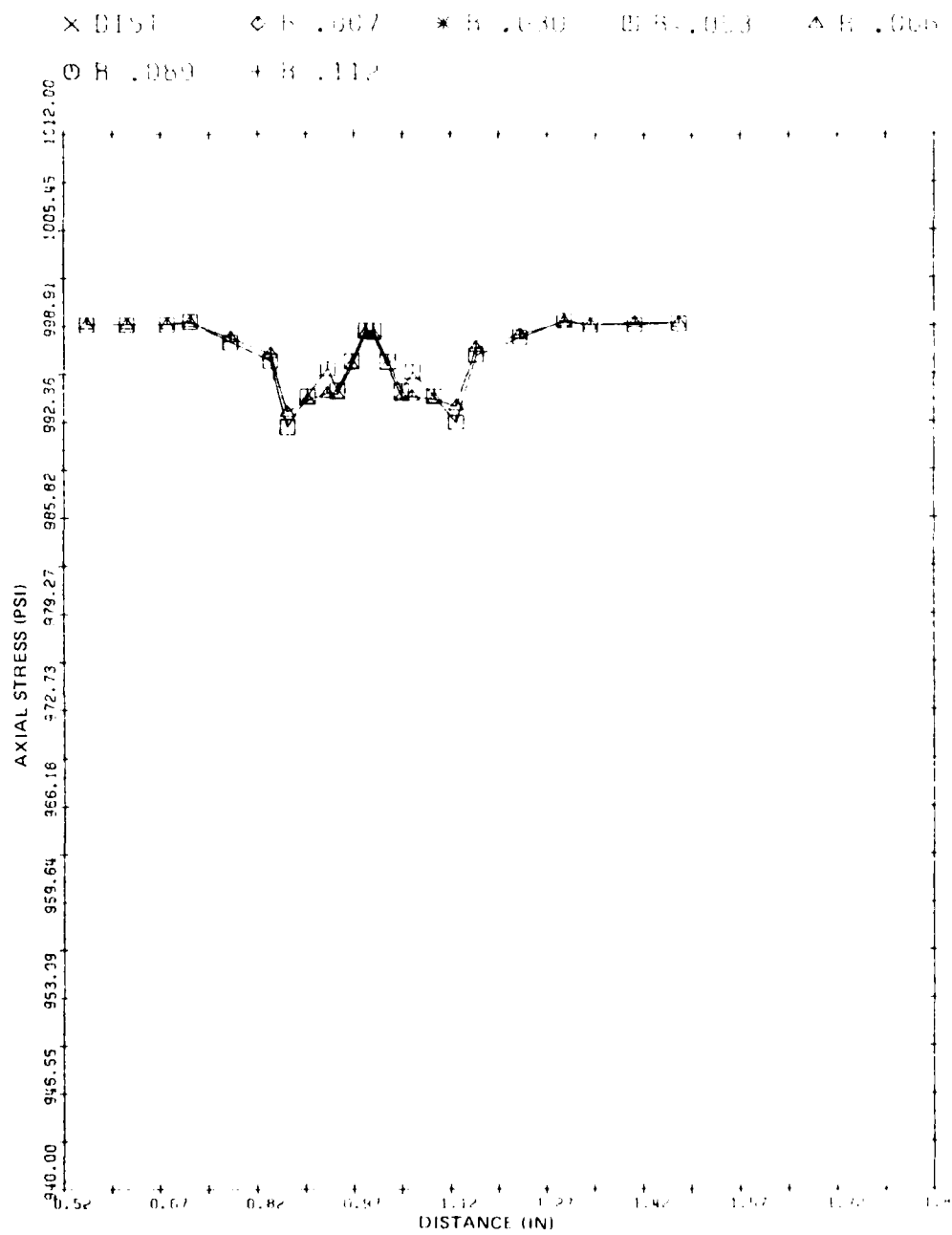
Figure 28. Axial stress plot at 15 degrees, one.

Figure 29. Axial stress plot at 15 degrees, mid-radius.

2/81 CD22629

Figure 30. Axial stress plot at 15 degrees, outer shell.
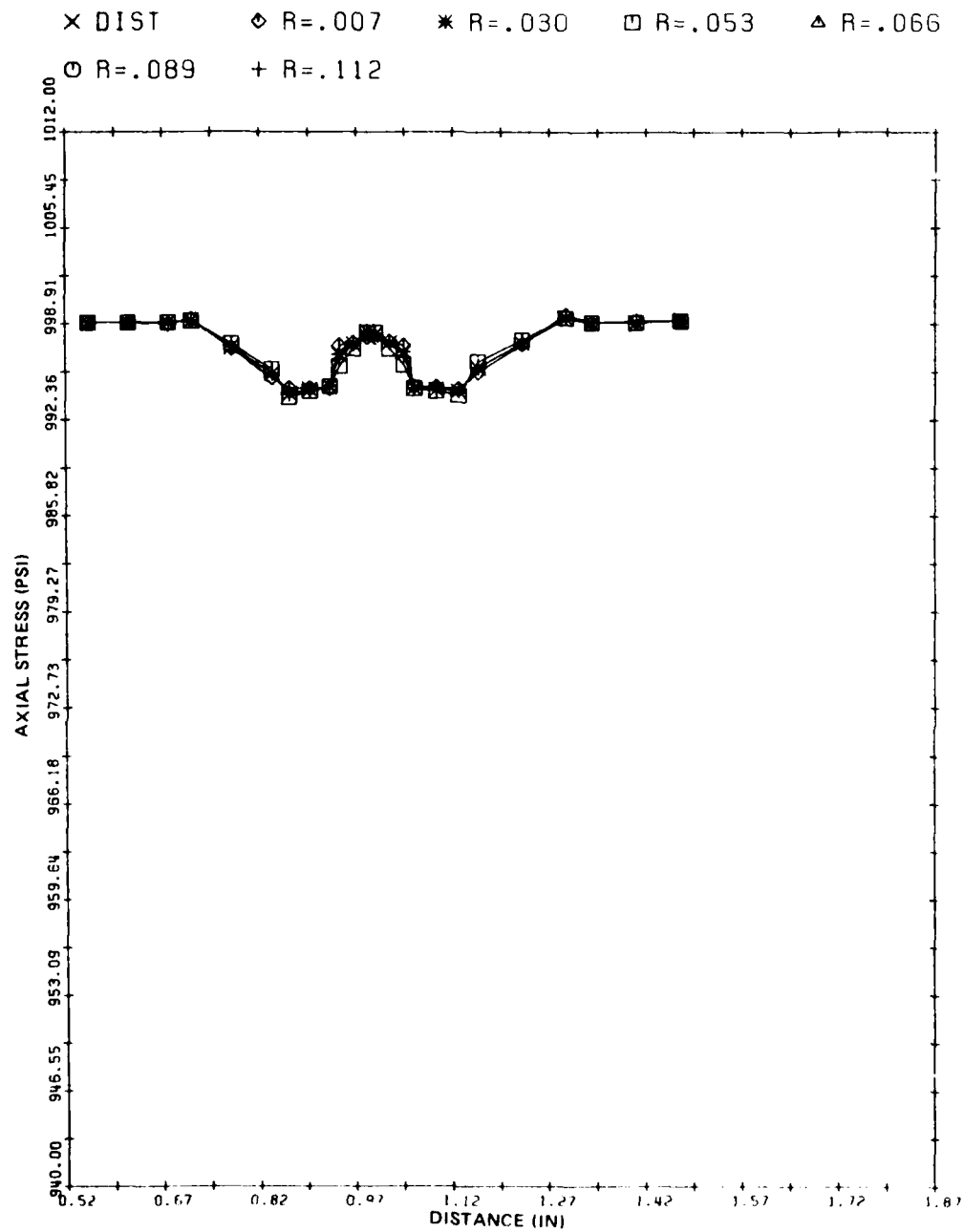
2/81 CD22630

Figure 31. Axial stress plot at 50 degrees, core.
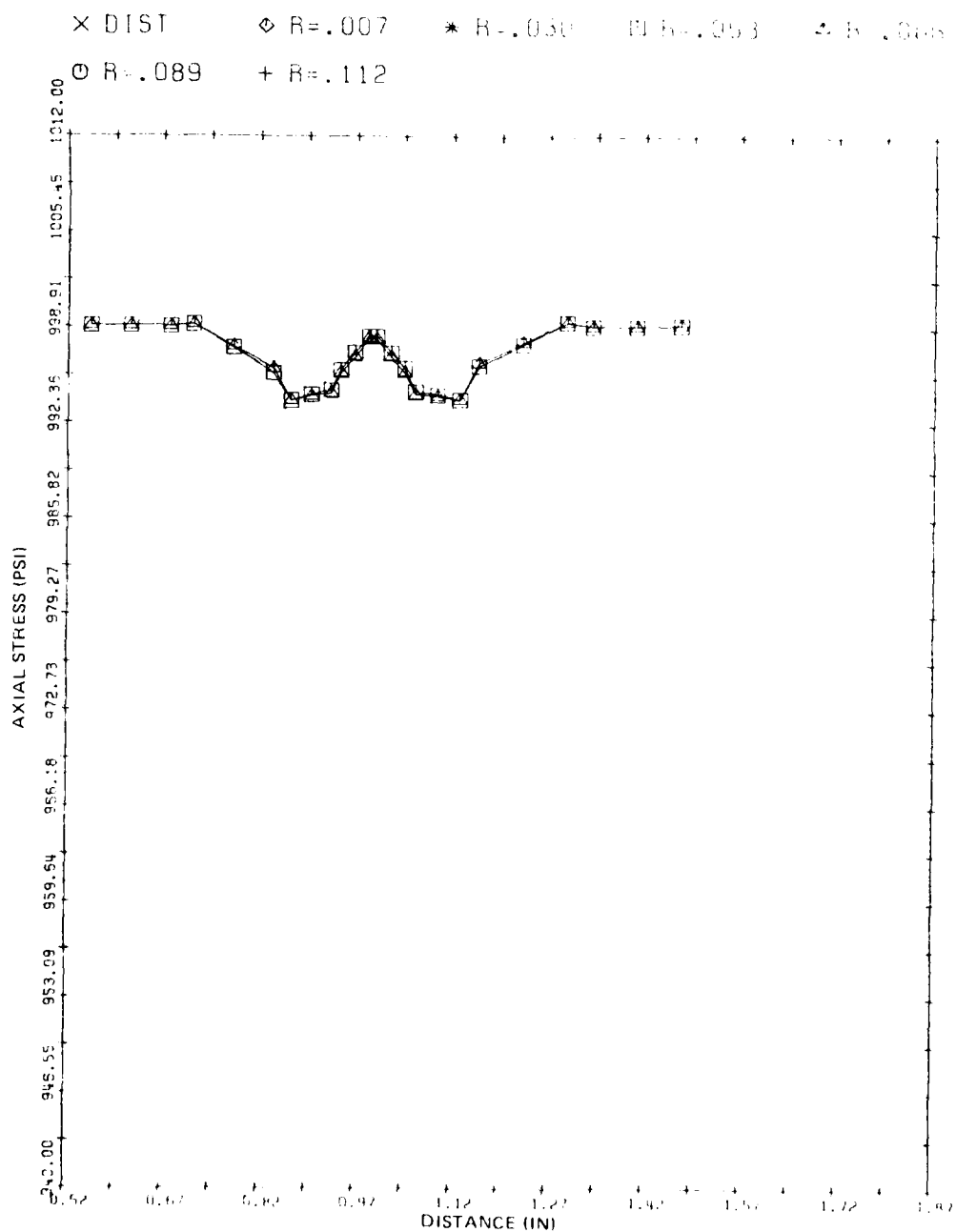
2/81 CD22631

Figure 32. Axial stress plot at 50 degrees, mid-radius.
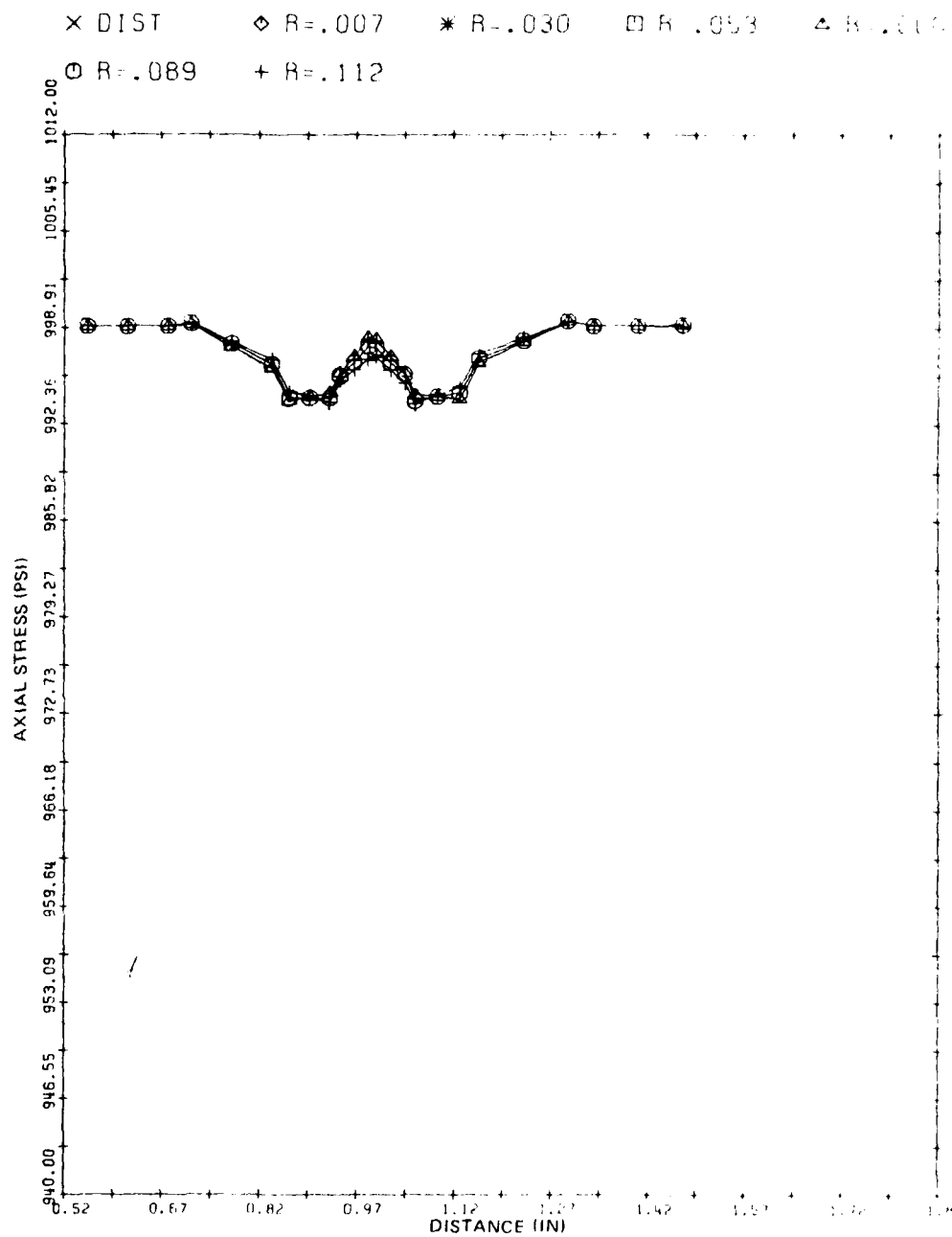
Figure 33. Axial stress plot at 50 degrees, outer shell.

2/81 CD22633

of radial location 0.112 and 0.089. However, these values are still within 1.2 percent of the nominal value for uniform stress. The plots in [illegible] again in [illegible] demonstrate a dramatic improvement over the a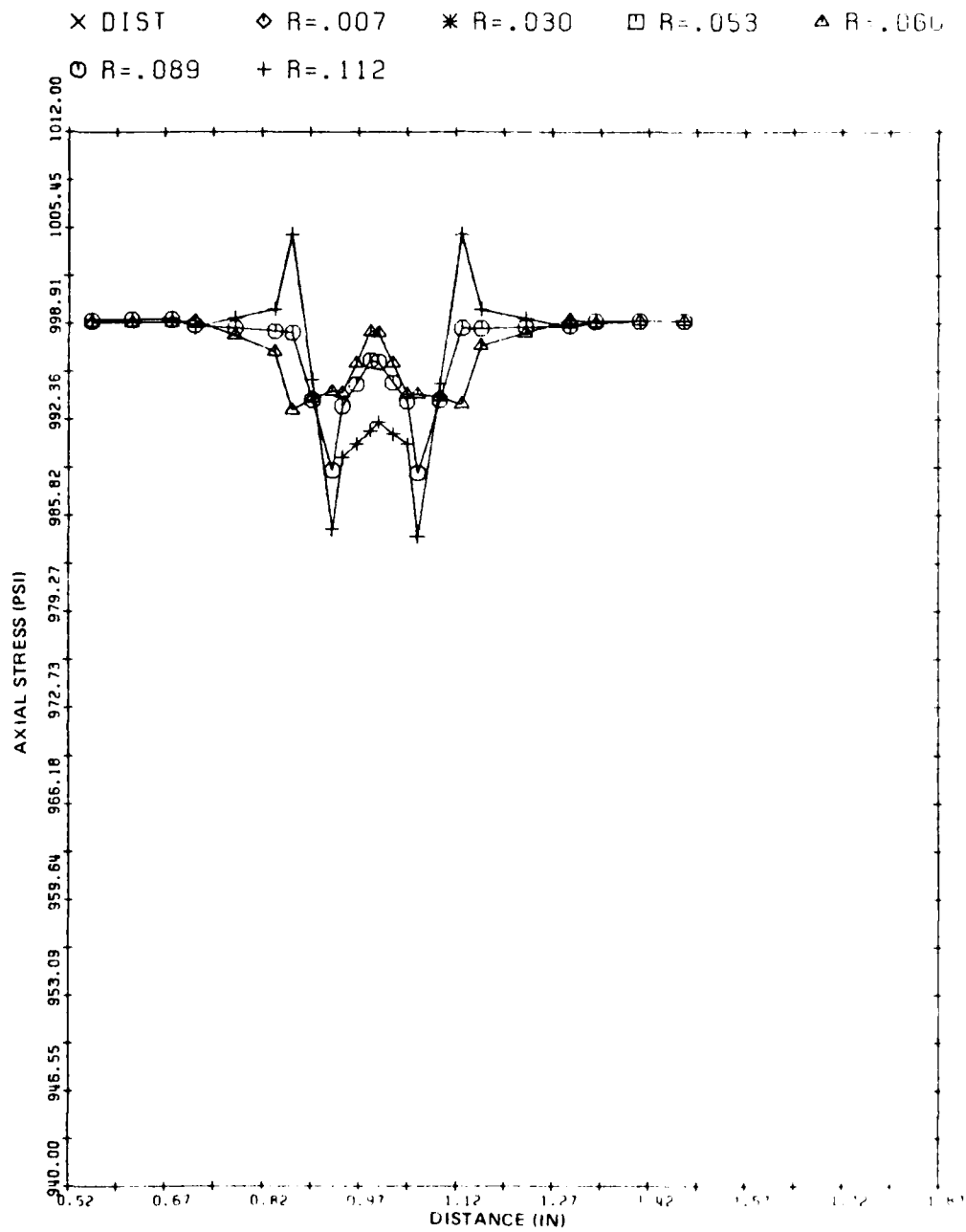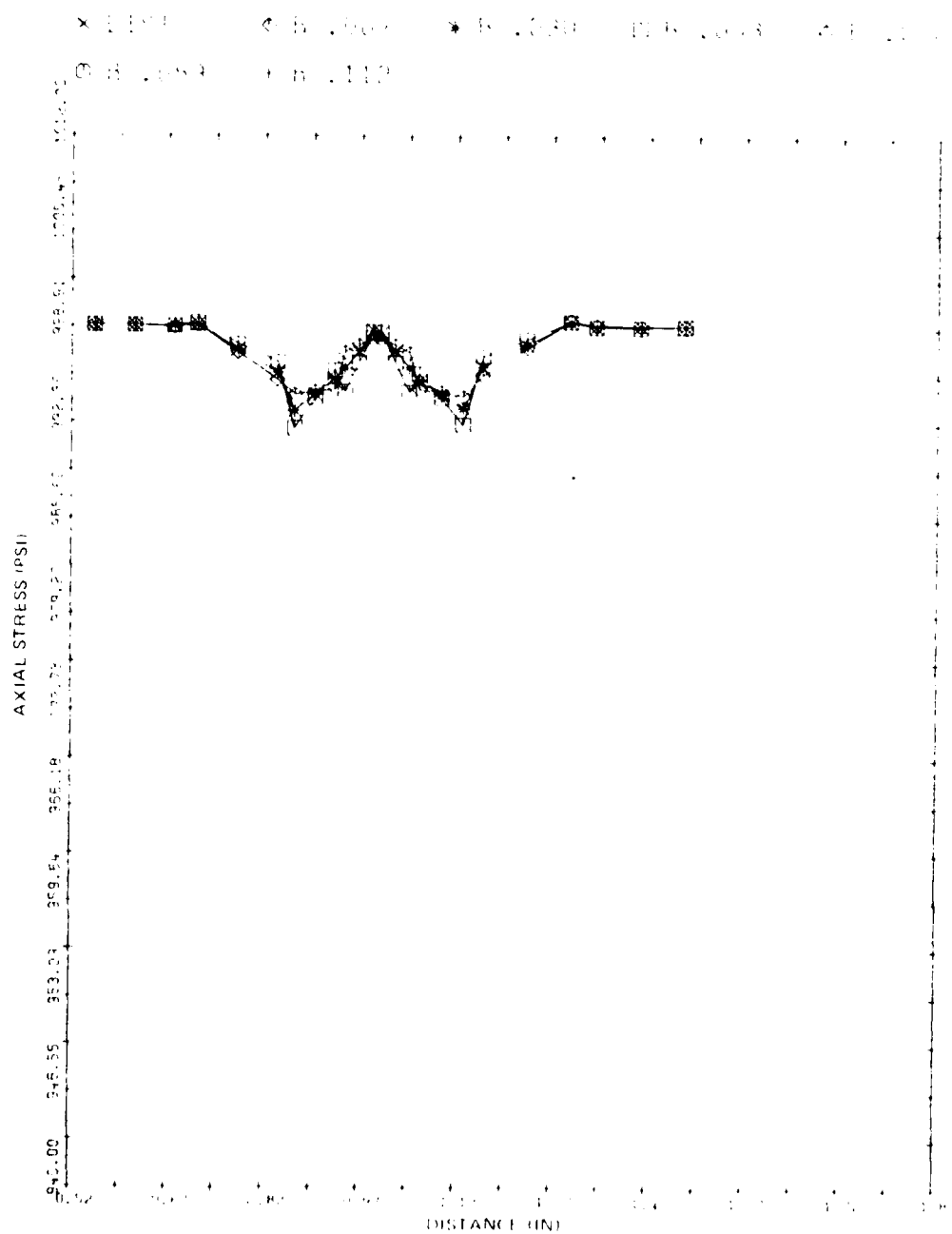xisymmetric case. The conclusion from this study is that stress level for this type of design is very similar to the axisymmetric design directly in the lug area, but much more uniform almost immediately away from it.

As an additional indication of the improvement of this design over the axisymmetric design, the axial displacement at the center of the lug for both designs are compared against the theoretical result for a perfectly cylindrical specimen with a 100-pound load. The results are tabulated in Table III.

Table III. Comparison of axial displacement at the center of support for two specimen designs.

Specimen Design	Displacement (inches)	Percent Error
Perfect cylinder	1.1353	---
Axisymmetric rib	1.1266	0.77
Lugged specimen	1.1336	0.15

The improvement obtained through use of the lugged specimen design is more than a factor of five.

4.5.2.4   Effect of Capacitor Plate Assembly Weight

Each of the lugs will support approximately 1/3 of the weight of the capacitor plate assembly. Although the exact weight is not known at this time, one pound was assumed for purposes of analysis. This is a reasonable estimation of the weight for the heavier of the two assemblies, and stresses may be scaled linearly when more exact information becomes known. Based on this assumption an axial load of .333 lbs. was applied at the center of the lug in the axial direction.

Figure 34 shows contours of Mises stresses through the lug section.
Peak stresses occur under the point load applied at the center. These
may be simulating Hertzian contact stresses under points of actual
contact between the lug and the clamp. However, they should be of no
concern because any creep produced by high values will disappear as the
contact area enlarges. Of greater concern are the stresses created near
the lug-cylinder interface. From Figure 34 these produce peak values of
366 lb/in^2. This stress is judged to be small enough not to create
detectable microcreep movement, but efforts will nevertheless be made to
reduce the weight of the capacitor plate assembly below 1 pound total.

4.5.3 Conclusions

(1) We have demonstrated in this study the limitations inherent
in using the conventionally defined microyield strength as
an indication of long-term microcreep behavior in as-
received and thermally treated HIP-50 beryllium. A more
correct interpretation of material response to applied
stresses, in the low strain regime, requires due
consideration of the strain exponent (obtained as the slope
of the straight line generated by plotting the microyield
data on logarithmic coordinates) in addition to the
calculated intercept of this straight line with the vertical
axis at a given, very low, value of residual strain (say
10^{-10}). We have interpreted this calculated value as
indicative of an intrinsic strength of the material and the
strain exponent as a measure of the processes of strain
hardening occurring in the material. The validity of such
an interpretation, however, depends on the assumption that
the linear relationship observed in the 10^{-6} strain regime
remains unchanged for even lower strain values (at least
down to the selected 10^{-10} strain).
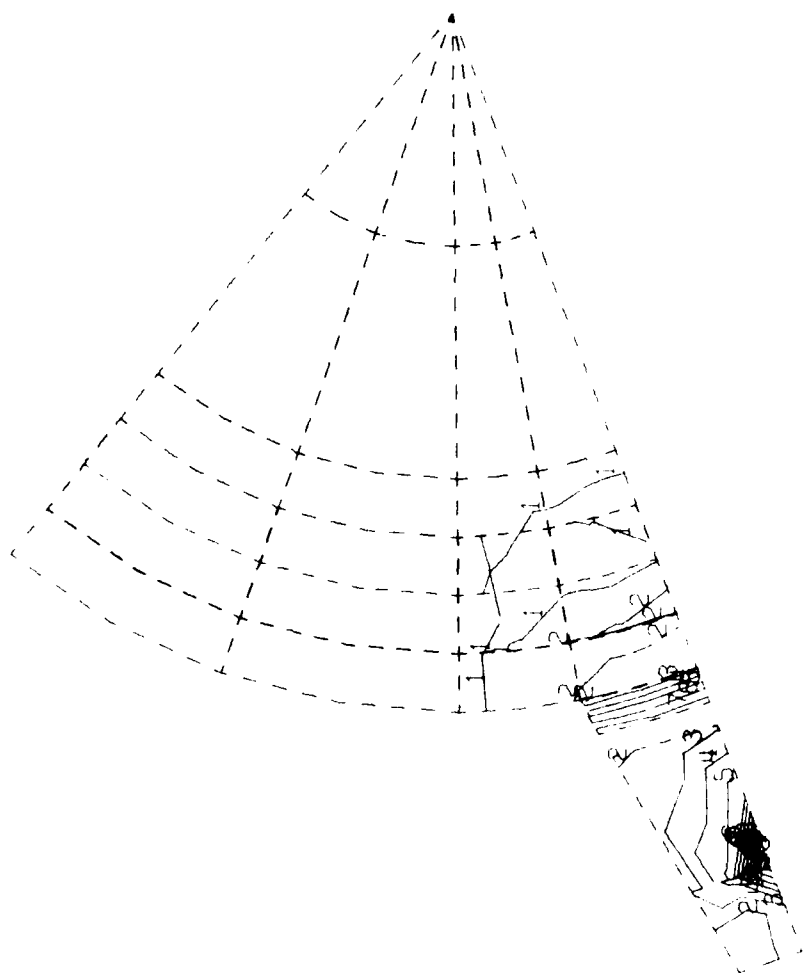
61

(2)   Optical microscopic examination of the as-HIP and the
        thermally treated materials failed to show significant,
        observable changes in microstructure that could be related
        to the measured variations in micromechanical properties.
        It was, however, determined that extreme care needs to be
        exercised in the preparation of samples from these materials
        in order to avoid the introduction of mechanical damage into
        the samples from improper sectioning and grinding
        procedures. This damage appeared as twins suggestive of
        stress relief at the mechanically polished surface in some
        of the samples.

(3)   Electron microscopic observation of suitably prepared foil
        samples provided substantially more insight into changes in
        sample microstructure that resulted from the heat treatments
        employed. The observed changes were mostly related to phase
        precipitation and segregation. In most instances these
        precipitates were very fine and could not be identified
        using the electron diffraction technique. Some, but not
        all, of the changes observed in micromechanical behavior of
        this material (from the selected thermal treatments) could
        be explained on the basis of these electron microscopic
        observations. The foil samples were successfully prepared
        using the jet-polishing technique with a chromic-acetic
        solution as the electrolyte.

(4)   Finite element analysis in this report has shown that creep
        test specimens with lugs to support the measurement
        fixturing will have markedly improved stress field
        uniformity compared to the conventional designs using
        axisymmetrical supports.

SECTION 5

RECOMMENDATIONS FOR FUTURE WORK

        To develop greater understanding of micromechanical processes,
the following need to be investigated.

    (1) Correlation of microcreep behavior with microyield and
         macroyield behavior.

    (2) Correspondence between microcreep behaviors measured in
         tension and compression.

    (3) Microstructure dependence of microcreep.

    (4) Examination of candidate materials, other than HIP-50
         beryllium.

    (5) Extended finite element modelling studies with new data.

References

(1)   Marschall, C.W., and R.E. Maringer, _Dimensional Instability - An Introduction_, Pergamon Press, 1977.

(2)   Polvani, R., National Bureau of Standards (NBS), Gaithersburg, Maryland (_private communication_).

(3)   McCarthy, J., and F. Petri, _Materials Research for Advanced Inertial Instrumentation, Task 1: Dimensional Stability of Gyro Structural Materials_, Charles Stark Draper Laboratory, Inc., Report R-1231, September 1978.

(4)   McCarthy, J., and F. Petri, _Materials Research for Advanced Inertial Instrumentation, Task 1: Dimensional Stability of Gyro Structural Materials_, Charles Stark Draper Laboratory, Inc., Report R-1388, June 1980.

(5)   Paine, R.M., and A.J. Stonehouse, _Investigation into Effects of Microalloying and Thermal Treatment on the Properties of Beryllium_, Final Report on Contract N60921-72-C-028, Brush-Wellman, Inc., Report BW-TR-549, Cleveland, Ohio, 1974.

BASIC DISTRIBUTION LIST

ORGANIZATION	COPIES	ORGANIZATION	COPIES
Defense Documentation Center Cameron Station Alexandria, VA 22314	12	Naval Air Propulsion Test Center Trenton, NJ 08628 ATTN: Library	1
Office of Naval Research Department of the Navy 800 N. Quincy Street Arlington, VA 22217	1	Naval Construction Battalion Civil Engineering Laboratory Port Hueneme, CA 93043 ATTN. Materials Division	1
ATTN: Code 471 Code 102 Code 470	1 1 1	Naval Electronics Laboratory San Diego, CA 92152 ATTN: Electron Materials Sciences Division	1
Commanding Officer Office of Naval Research Branch Office Building 114, Section D 666 Summer Street Boston, MA 02210	1	Naval Missile Center Materials Consultant Code 3312-1 Point Mugu, CA 92041	1
Commanding Officer Office of Naval Research Branch Office 536 South Clark Street Chicago, IL 60605	1	Commanding Officer Naval Surface Weapons Center White Oak Laboratory Silver Spring, MD 20910 ATTN: Library	1
Office of Naval Research San Francisco Area Office 760 Market Street, Room 447 San Francisco, CA 94102	1	David W. Taylor Naval Ship Research and Development Center Materials Department Annapolis, MA 21402	1
Naval Research Laboratory Washington, DC 20375		Naval Undersea Center San Diego, CA 92132 ATTN: Library	1
ATTN: Code 6000 Code 6100 Code 6300 Code 6400 Code 2627	1 1 1 1 1	Naval Underwater System Center Newport, RI 02840 ATTN: Library	1
Naval Air Development Center Code 302 Warminster, PA 18964 ATTN: Mr. F. S. Williams	1	Naval Weapons Center China Lake, CA 93555 ATTN: Library	1
		Naval Postgraduate School Monterey, CA 93940 ATTN: Mechanical Engineering Department	1

69

BASIC DISTRIBUTION LIST (continued)

ORGANIZATION	COPIES	ORGANIZATION	COPIES
Naval Air Systems Command Washington, DC 20360 ATTN: Code 52031 Code 52032	 1 1	NASA Headquarters Washington, DC 20546 ATTN: Code RRM	1
Naval Sea System Command Washington, DC 20362 ATTN: Code 035	1	NASA (216) 433-4000 Lewis Research Center 21000 Brookpark Road Cleveland, OH 44135 ATTN: Library	1

Naval Facilities Engineering
   Command
Alexandria, VA 22331
ATTN: Code 03
	1	National Bureau of Standards
		Washington, DC 20234
		ATTN: Metallurgy Division
		        Inorganic Materials Division
			1

Scientific Advisor Commandant of the Marine Corps Washington, DC 20380 ATTN: Code AX	1	Director Applied Physics Laboratory University of Washington 1013 Northeast Fortieth Street Seattle, WA 98105	1
Naval Ship Engineering Center Department of the Navy Washington, DC 20360 ATTN: Code 6101	1	Defense Metals and Ceramics Information Center Battelle Memorial Institute 505 King Avenue Columbus, OH 43201	1
Army Research Office P.O. Box 12211 Triangle Park, NC 27709 ATTN: Metallurgy and Ceramics Program	1	Metals and Ceramics Division Oak Ridge National Laboratory P.O. Box X Oak Ridge, TN 37380	1
Army Materials and Mechanics Research Center Watertown, MA 02172 ATTN: Research Programs Office	1	Los Alamos Scientific Laboratory P.O. Box 1663 Los Alamos, NM 87544 ATTN: Report Librarian	1

Air Force Office of Scientific
   Research
Bldg. 410
Bolling Air Force Base
Washington, DC 20332
ATTN: Chemical Science Directorate
        Electronics and Solid State
          Sciences Directorate
	1	Argonne National Laboratory
		Metallurgy Division
		P.O. Box 229
		Lemont, IL 60439
			1

ORGANIZATION	COPIES	ORGANIZATION	COPIES
Air Force Materials Laboratory Wright-Patterson AFB Dayton, OH 45433	1	Brookhaven National Laboratory Technical Information Division Upton, Long Island New York 19973 ATTN: Research Library	1
Library Building 50, Rm 134 Lawrence Radiation Laboratory Berkeley, CA	1	Office of Naval Research Branch Office 1030 East Green Street Pasadena, CA 91106	1

Dr. Bruce W. Christ
Division 562
National Bureau of Standards
325 S. Broadway
Boulder, CO 80303

Dr. Robert S. Polvani
Room B-120, Materials Bldg.
National Bureau of Standards
Washington, D.C. 20234

Dr. A. W. Ruff, Jr.
National Measurement Laboratory
National Bureau of Standards
Washington, DC 20234

Dr. Robert Hocken
Room B-104, Metrology Bldg.
National Bureau of Standards
Washington, D.C. 20234

Dr. Gilbert J. London
Code 2023
Naval Air Development Center
Warminster, PA 18974

Professor G. S. Ansell
Rensselaer Polytechnic Institute
Dept. of Metallurgical Engineering
Troy, NY 12181

Professor J. B. Cohen
Northwestern University
Dept. of Material Sciences
Evanston, IL 60201

Professor M. Cohen
Massachusetts Institute of Technology
Department of Metallurgy
Cambridge, MA 02139

Professor J. W. Morris, Jr.
University of California
College of Engineering
Berkeley, CA 94720

Professor O. D. Sherby
Stanford University
Materials Sciences Division
Stanford, CA 94300

Dr. E. A. Starke, Jr.
Georgia Institute of Technology
School of Chemical Engineering
Atlanta, GA 30332

Professor David Turnbull
Harvard University
Division of Engineering and
  Applied Physics
Cambridge, MA 02139

Dr. D. P. H. Hasselman
Montana Energy and MHD Research
  and Development Institute
P.O. Box 3809
Butte, MT 59701

Dr. L. Hench
University of Florida
Ceramics Division
Gainesville, FL 32601

Dr. J. Ritter
University of Massachusetts
Department of Mechanical Engineering
Amherst, MA 01002

Professor G. Sines
University of California, Los Angeles
Los Angeles, CA 90024

Director
Materials Sciences
Defense Advanced Research Projects
  Agency
1400 Wilson Boulevard
Arlington, VA 22209

Professor H. Conrad
University of Kentucky
Materials Department
Lexington, KY 40506

Dr. A. G. Evans
Dept. Material Sciences and
  Engineering
University of California
Berkeley, CA 94720

Professor H. Herman
State University of New York
Materials Sciences Division
Stoney Brook, NY 11794

Professor J. P. Hirth
Ohio State University
Metallurgical Engineering
Columbus, OH 43210

Professor R. M. Latanision
Massachusetts Institute of Technology
77 Massachusetts Avenue
Room E-19-702
Cambridge, MA 02139

Dr. Jeff Perkins
Naval Postgraduate School
Monterey, CA 93940

Dr. R. P. Wei
Lehigh University
Institute for Fracture and
  Solid Mechanics
Bethlehem, PA 18015

Professor H. G. F. Wilsdorf
University of Virginia
Department of Materials Science
Charlottesville, VA 29903

Mr. Robert C. Fullerton-Batten
Kawecki Berylco Industries, Inc.
P.O. Box 1462
Reading, PA 19603

Mr. Norman Pinto
Kawecki Berylco Industries, Inc.
P.O. Box 1462
Reading, PA 19603

A. G. Gross
Mechanical Metallurgy Unit
Autonetics, Inc.
Anaheim, CA

A. J. Stonehouse
The Brush Beryllium Co.
Cleveland, OH

C. W. Marschall
Columbus Laboratories
Battelle Memorial Institute
Columbus, OH

R. E. Maringer
Columbus Laboratories
Battelle Memorial Institute
Columbus, OH

J. E. Hanafee
Lawrence Livermore Laboratory
University of California
Livermore, CA 94550

Dr. Frank Gardner
Acting Scientific Director
Office of Naval Research
Building 114-Section D
666 Summer Street
Boston, MA 02210

Dr. Phil Clarkin
Metallurgy and Ceramics
Office of Naval Research
6th Floor, Room 619
800 N. Quincy Street
Arlington, VA 22217

Mr. George Keith
Kawecki Berylco Industries, Inc.
P.O. Box 1462
Reading, PA 19603

Mr. Bruce Borchardt
Room B-104, Metrology Bldg.
National Bureau of Standards
Washington, D C. 20234

Mr. Tom Charlton
Room B-104, Metrology Bldg.
National Bureau of Standards
Washington, D.C. 20234